Basin Research

IAS EAGE

Basin Research (2015) 1–25, doi: 10.1111/bre.12163

Isotopic and thermochronologic evidence of extremely cold lithosphere associated with a slab flattening in the Central Andes of Argentina

Gilda Collo,* Federico M. Dávila,* Wilson Teixeira,† Julieta C. Nóbile,* Lucy G. Sant′ Anna‡ and Andrew Carter§

**Centro de Investigaciones en Ciencias de La Tierra, CONICET-UNC, Córdoba, Argentina*
†*Institute of Geosciences, University of São Paulo, São Paulo, SP, Brazil*
‡*School of Arts, Sciences and Humanities, Institute of Energy and Environment, University of São Paulo, São Paulo, SP, Brazil*
§*Department of Earth and Planetary Sciences, Birkbeck University of London, London, UK*

ABSTRACT

We present mineralogic, isotopic and thermochronologic analyses on psammopelitic and tuffaceous levels from the Bermejo and Vinchina basins – both foreland depocentres of the Central Andes of Argentina – that define a low-temperature regime for the crust akin to a slab shallowing and flattening process. The contents of illite in illite/smectite interstratified (I/S) show a progressive illitization into the deeper parts of both basins. The distribution of I/S is compatible with theoretical simulations and predicted heat flow values of *ca*. 26 mW m^{-2} in the 8–3.4 Ma interval for the Vinchina Basin and *ca*. 42 mW m^{-2} since 9 Ma for the Bermejo Basin. The latter shows heat flow values that are comparable to those reported by magnetotelluric analysis (36–40 mW m^{-2}) in agreement with previously published heat flow calculations along the modern Andean foreland. The Rb–Sr isochrones in psammopelites (<2 μm fractions) show ages between 125 and 165 Ma, whereas the K–Ar ages decrease as the grain size is smaller (136–224 Ma for 1–2 μm, 112–159 Ma for 0.2–1 μm, 76–116 Ma for <0.2 μ and 39.3–42 Ma for <0.1 μm). These ages are significantly older than the sedimentation in the basins (*ca*. 16 Ma for the Vinchina Basin; U–Pb age), and can be explained by the presence of a significant amount of detrital components, mainly illite, even in the finer fractions. The preservation of detrital ages is consistent with the shallow diagenesis related to a low-temperature regime, proposed here for the basins. Younger K–Ar ages (21.3–12 Ma) were obtained for a basal tuffaceous level. Clay mineralogy and R0 ordering in the deepest part of the Vinchina Basin, together with the evolution model of I/S with depth, suggest that the burial temperatures would have not exceeded *ca*. 100°C in agreement with (U–Th)/He analyses performed on apatite extracted from two tuffaceous units. Thermal indicators from both studied basins confirm the existence of a low-temperature regime during flat subduction.

INTRODUCTION

The characterization of thermal regimes during the time-spatial interval allow a simple estimation of the temperatures reached by clastic basins, constituting a powerful tool to understand their mechanical and thermal properties, fundamental aspects in tectonic and geodynamic reconstructions. Hence, the mineralogical analyses on different clay fractions combined with their geochronology using various techniques coupled with low-temperature thermochronology are widely used for estimating the time of the maximum temperature, cooling and reheating episodes in sedimentary basins. In particular, palaeo-thermometry and thermochronology data from sedimentary successions may be useful to track temperature changes in time and space related to subsidence-exhumation history and possible heat flux changes. Such techniques have proven powerful tools for hydrocarbon exploration (Allen & Allen, 2005) as well as for basin and geodynamic modelling studies that require constraints on palaeo-heat flow and the palaeo-thermal state of local crust (Pollack *et al.*, 1993; Gutscher *et al.*, 2000; Husson & Moretti, 2002; Collo *et al.*, 2011).

Correspondence: Gilda Collo, Centro de Investigaciones en Ciencias de La Tierra, CONICET-UNC, Av. Vélez Sarsfield 1611, Ciudad Universitaria, X5016GCA, Córdoba, Argentina. E-mail: gildacoll@gmail.com

In this study, we used mineralogical and geochronological analyses of clay fractions, combined with apatite (U–Th)/He thermochronometry to define the thermal histories of Mio-Pliocene sedimentary rocks deposited in two foreland basins with a thick stratigraphic section located in the central Andes of Argentina, namely the Vinchina and Bermejo basins. Exposures within the Vinchina Basin, (Ramos, 1970; Jordan & Alonso, 1987) show >10 km of synorogenic strata along the thrust front, at the foothill of the Andes that were exhumed <3.5–4 Ma ago (Collo *et al.*, 2011 and references therein). Vinchina rocks can be correlated with subsurface successions in the 6-km thick Bermejo Basin (Jordan *et al.*, 1993; Fig. 1). The Vinchina Basin subsided during the Miocene flat slab regime (Anderson *et al.*, 2007) and was exhumed in the Pliocene when subduction became steeper along this segment (Fig. 1). By contrast Miocene deposition in the Bermejo Basin, took place during a normal subduction regime and today the basin is located above the flat slab segment (Fig. 1). Study of the palaeo-thermal regimes in these two basins offers an opportunity to examine if and how heat flow varied in time and space (along strike) in association with slab shallowing and flattening (Gutscher *et al.*, 2000; Husson & Moretti, 2002; Collo *et al.*, 2011; among others) considering that the Juan Fernández Ridge (considered the main mechanism for driving slab buoyancy Kay & Mpodozis, 2002) shifted southwards during subduction. In order to define burial and exhumation histories and improve understanding of the palaeo-thermal evolution of the Vinchina and Bermejo basins during the main period of Andean mountain building (i.e. last 20 million years) we dated volcaniclastic levels (zircon U–Pb geochronology), characterized the growth history of clay minerals (K–Ar and Rb–Sr) and applied low-temperature thermochronology (apatite (U–Th)/He) to samples from the deepest parts of the basin.

GEOLOGY OF THE VINCHINA AND BERMEJO BASINS

The Vinchina Basin

This synorogenic Neogene basin locally reaches a thickness of *ca*. 10 km. Outcrops are relatively continuous in the Sierra de los Colorados (28–30° LS) (Ramos, 1970), of the La Rioja province of the Central Andes in Argentina (see Fig. 1). The basin stratigraphy is represented by the Vinchina and Toro Negro formations (Turner, 1964; Fig. 2). Sedimentation occurred between the Early Miocene and Pliocene (Ciccioli *et al.*, 2005, 2014a,b; Collo *et al.*, 2011 and references therein). Magnetostratigraphic studies (Reynolds *et al.*, 1990; Re & Barredo, 1993) tied to zircon fission track ages on tuff levels (Tabbutt, 1986), as well as recent U–Pb chronology (Dávila *et al.*, 2008; Collo *et al.*, 2011, 2014; Ciccioli *et al.*, 2012, 2014b) constrain the deposition of sediments to between *ca*. 16 and *ca*. 3.4 Ma. Subhorizontal conglomerates unconformably lying on top of the dipping sequence of the Toro Negro

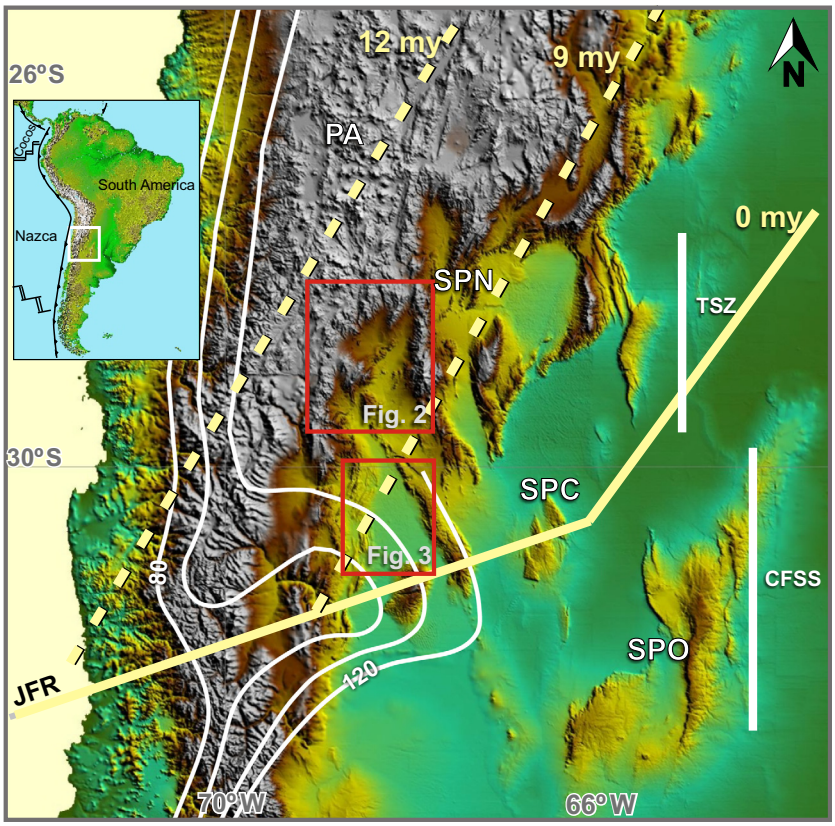

Fig. 1. Location of the basins. Topographic Image (U.S. Geological Survey) showing the foreland of the Central Andes of Argentina. The Vinchina (Fig. 2) and the Bermejo (Fig. 3) basins are indicated. It was further indicated the area affected by the current flat subduction segment (CFSS) and the transitional subduction zone (TSZ) (after Barazangi & Isacks, 1976). PA: Puna Austral; SPN: Sierras Pampeanas del Norte; SPC: Sierras Pampeanas Centrales, SPO: Sierras Pampeanas Orientales, JFR: Juan Fernández ridge. Modified from Collo *et al.* (2011).

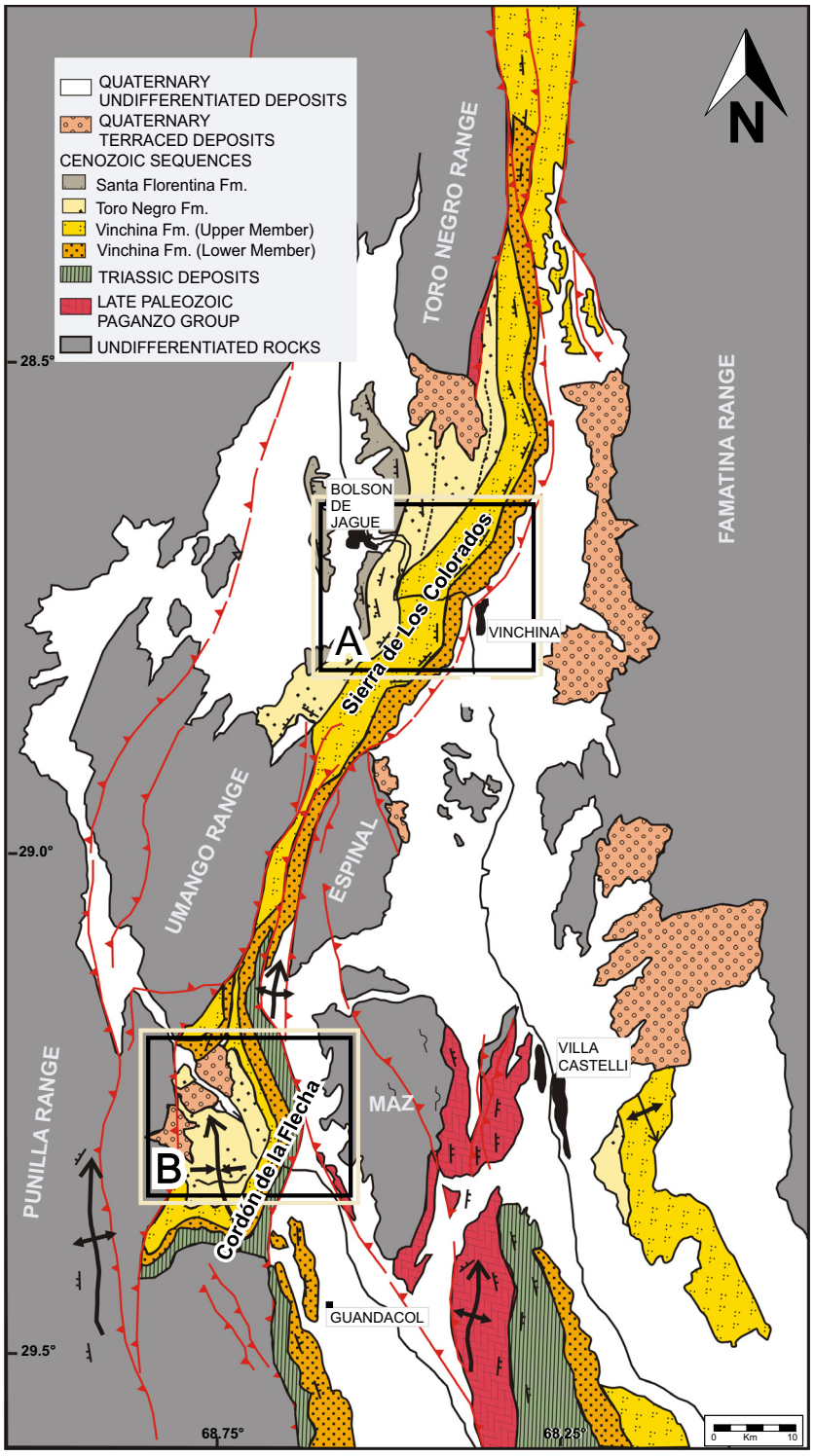

Fig. 2. Geological map of the western region of La Rioja province, showing distribution of Tertiary deposits in the Vinchina Basin (modified from Ramos, 1999). (a) Quebrada de la Troya norte section, (b) Quebrada de la Troya Sur section.

and Vinchina formations indicate that erosion and exhumation of the Vinchina Basin occurred after 3.4 Ma ago (youngest age of Toro Negro Formation). Although no radiometric ages are available for the horizontal conglomerates in the study area, equivalent units to the northeast (in Fiambalá, Punashotter conglomerates) were recently dated between 3.77 and 3.05 Ma (Carrapa *et al.*, 2008) and eastward ones (in Famatina, Santa Florentina Formation) were biostratigraphically constrained to the Plio-Pleistocene (Lencinas, 1994). These ages indicate that Vinchina Basin sedimentation lasted *ca*. 16 myr and the residence time at maximum burial was short-lived before its exhumation.

The Bermejo Basin

This basin is located to the south of the Vinchina Basin and mainly outcrops along the Eastern Precordillera

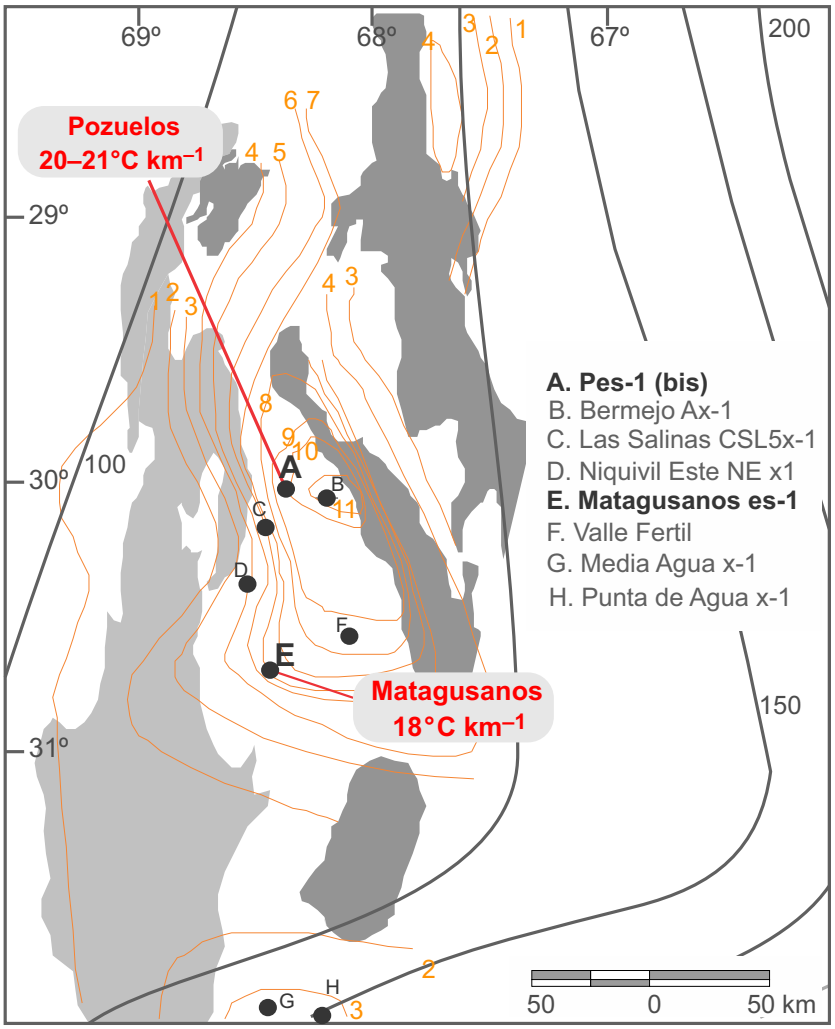

Fig. 3. Isopachic map of the main syn-orogenic depocentres from the Andean cycle in the central-northern Precordillera Region (San Juan and La Rioja Provinces). Pozuelos and Matagusanos boreholes are located (modified from Astini *et al.*, 2005).

(30–33° LS, Fig. 1) except between the Precordillera and the Sierra de Valle Fértil where the sequence remains buried (Fig. 3). Although the stratigraphy is known, mainly by outcrop studies (see Jordan *et al.*, 1993, 2001; Milana *et al.*, 2003; and references therein), seismic interpretations and borehole studies (Zapata & Allmendinger, 1996) have allowed the correlation and comparison with other synorogenic basins along the Andes, such as the Vinchina Basin. The Bermejo stratigraphy has been divided into three formations named Huachipampa, Quebrada del Cura and Rio Jachal (Jordan *et al.*, 1993). Although parts of the basin have been affected by thrusting, most boreholes show a continuous Tertiary sequence *ca*. 6000-m thick (Fig. 4). The basin history is similar to Vinchina, consistent with eastward Andean foreland migration since *ca*. 20 Ma ago (Jordan *et al.*, 1993, 2001). Jordan *et al.* (2001) recognized three main sedimentation stages across this basin: The first two, between 20 and 7 Ma, associated with the evolution of a flexural foreland, mainly controlled by the Cordilleran loading by thrusting, and a third stage that would correspond to a broken foreland, from 7 Ma to present.

In both basins, deposition, burial and exhumation occurred during a single orogenic phase, in association with thrust migration and widening of the Cordillera and Precordillera thrust belt (Jordan *et al.*, 2001). Today, the Vinchina Basin places within the northern transitional zone with respect to the flat slab segment of Chile–Argentina (Fig. 1). However, the burial history would have occurred during a stage of flat subduction (Kay & Mpodozis, 2002; Dávila & Astini, 2007). The correlative Bermejo Basin would have occupied a transitional segment during the Late Miocene, located over the flat slab since that time (by comparison with the Kay & Mpodozis, 2002 model).

THEORETICAL FRAMEWORK

The evolution of clay minerals helps in understanding the palaeo-thermal history of a region as the percentage of smectite in interstratified I/S from clastic sequences and the appearance of illite and white mica are a proxy of the maturity of a basin and the geothermal gradients prevailing during the burial of a succession (e.g. Arostegui *et al.*, 2006; Nieto & Abad, 2007; Srodon, 2007). The proportion of smectite in interstratified I/S decreases with depth and, where the geothermal gradients are well known, changes in expandability of I/S and temperature can be

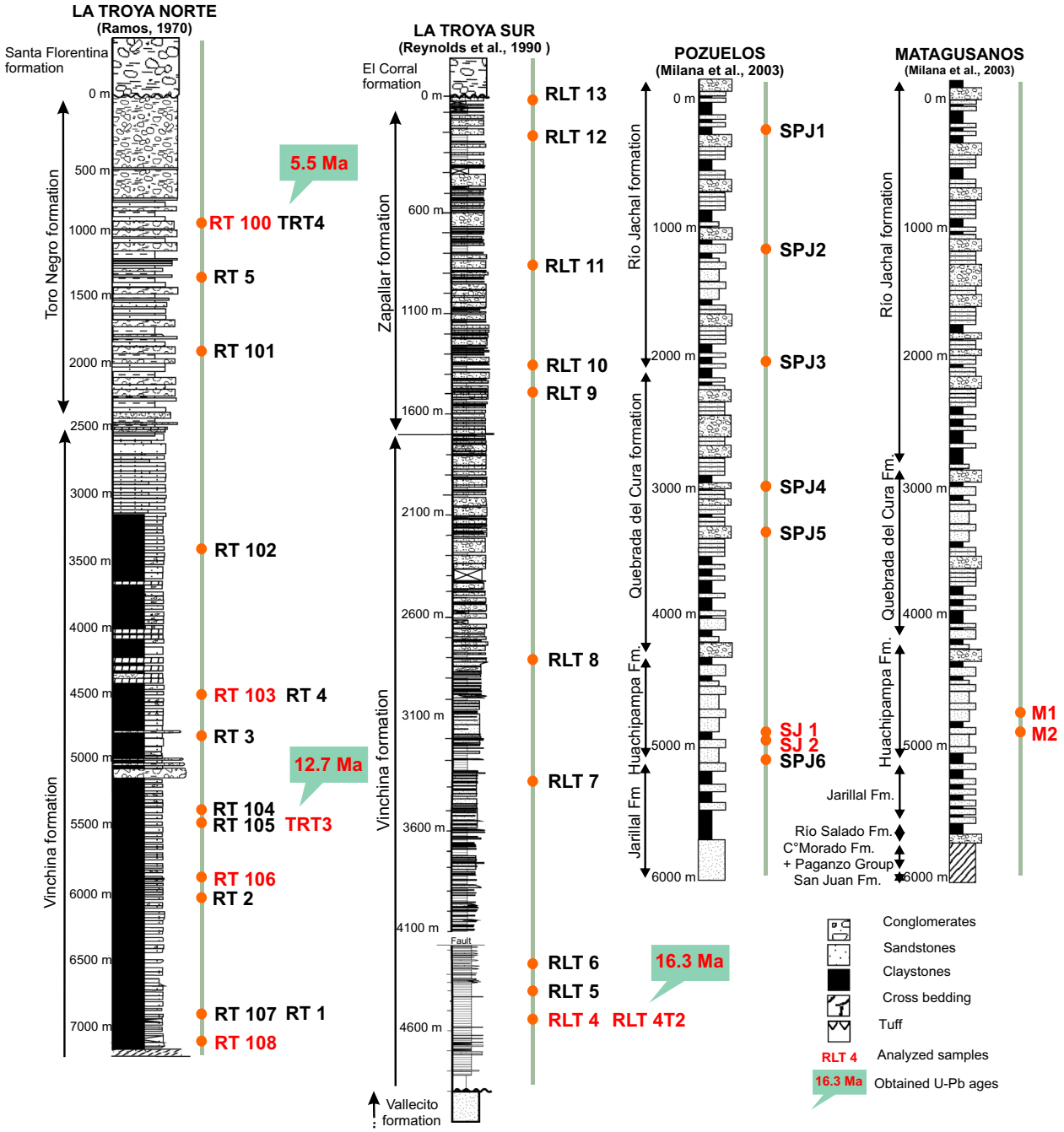

Fig. 4. Schematic stratigraphic columns of the studied sections. With interpretative purposes and comparisons between subsurface and outcrops, the columns are shown as "boreholes" i.e. zero level to the top and maximum thicknesses to the bottom (Modified from Ramos, 1970; Reynolds *et al.*, 1990 and Milana *et al.*, 2003). Analysed samples (red) and obtained U–Pb ages are shown.

associated. For instance, under high-thermal gradients, >40°C km^{-1} (e.g. South Central Texas basin, Velde & Vasseur, 1992; Awwiller, 1993), the content of smectite in the I/S decreases promptly, reaching concentrations of <50% at 2.5-km depth. In contrast, in basins subjected to low-gradients, <25°C km^{-1} (e.g. Shimiogarshi and Los Angeles basins; Velde & Vasseur, 1992), >50% smectite in I/S remains at 5-km depth. Consequently, illitization progress along the sedimentary record allows a simple inference of the palaeo-temperatures reached by the basins.

The isotopic characterization of clay minerals, in turn, allows assigning an age to each of the identified mineral growth episode, such as in K–Ar and Rb–Sr analyses. As burial and temperature increase in sedimentary basins, clay minerals begin to grow and, if the succession does not exceed the closure temperatures of the system, the ages obtained by the K–Ar method reflect the time that K^+ has been in crystal from its growing. Because in clay minerals a complete loss of ^{40}Ar occurs at *ca.* 260 ± 30°C (Hunziker *et al.*, 1986), ages of newly formed phases can be obtained from those samples that have not exceeded

the anchizone–epizone field. Moreover, a consistent interpretation of the isotopic results depends on a proper characterization of the mineral fraction to be analysed. Different neoformed clay mineral phases represent different genetic events in the mineral evolution of a succession, so the separation and characterization of that fractions with grain sizes <2 μm and of several different sub-fractions is substantial (Uysal, 1999; Uysal *et al.*, 2000; Clauer, 2007). The effect of contamination due to the presence of detrital phases carrying K^+ (see Clauer & Chaudhuri, 1999) should also be tested. For a successful isotopic dating, it is essential that any K^+ carrying particle, with the exception of authigenic clay minerals, is not present in the fraction analysed. This premise is difficult to achieve because most of the clay size fraction separated from the whole rock is heterogeneous. In this regard, the function that explains the relationship between detrital–authigenic mixed ages can be obtained from the correlation between these ages and the absolute (Środoń, 1999) or relative (Pevear, 1992) concentrations of detrital and authigenic components from different clay phases. Ages may also be related to the chemical composition of the analysed phases, assuming the concentration of some elements such as Na+, has a direct relationship with the proportion of detrital grains (Sant' Anna *et al.*, 2006). Another complexity is related with the amount of radiogenic argon accumulated in younger samples, which is significantly low. In these cases the "Peak comparison method" allows detecting small amounts of radiogenic ^{40}Ar diluted by ^{40}Ar from atmospheric contamination. This method compares the signal of ^{40}Ar extracted from an aliquot of the sample to a signal of the same level measured from pure atmosphere under rigorously identical analytical conditions (Gillot *et al.*, 2006 and references therein).

As illite clay minerals contain Rb, the Rb–Sr system is also frequently used for dating. The partial or complete homogenization of the Rb–Sr system during the burial history of a succession takes place in the anchizone–epizone interval (200–300°C; Cordani *et al.*, 1978, 2004). Consequently, below the anchizone this system behaves like the K–Ar system. To obtain diagenetic ages, the best results are supplied by "internal isochronous", constructed from analyses of authigenic fractions (<2 μm), leachates (with dilute HCl) and residues (Cordani *et al.*, 2004).

Low-temperature thermochronology, such as the (U–Th)/He system and fission tracks in apatite and zircon, allows constraining the time-temperature history for different rock types in near-surface conditions (<10 km) (Reiners *et al.*, 2005). These methods are commonly used to constrain the time, amount and rate of cooling/exhumation associated with mountain building, crustal deformation and extensional tectonic (e.g. Brown *et al.*, 1994; Ehlers & Farley, 2003; Fitzgerald *et al.*, 1995; Farley *et al.*, 1996 Stockli *et al.*, 2003). Given that this method records the thermal history of mineral grains, providing time–temperatures, it also allows interpreting the heating/burial rates of sedimentary accumulations that underwent diagenesis. This technique constitutes an extraordinary complement for the previously described isotopic techniques (K–Ar and Rb–Sr). In general, the He in apatites is retained at temperatures below 40°C and is removed from the crystal at temperatures as low as 80°C (Wolf *et al.*, 1996; Flowers *et al.*, 2009). This range of temperature (40–80°C) is known as the He partial retention zone (HePRZ) in apatite.

SAMPLING AND ANALYTICAL PROCEDURES

The Vinchina Basin was sampled across the Sierra de Los Colorados along two main creeks, the Quebrada de la Troya Norte (*ca*. 7-km thick) to the north and Quebrada de la Troya Sur (*ca*. 5-km thick; Figs 2 and 4) to the south. Twenty-four psammopelitic and volcaniclastic levels were sampled every *ca*. 500 m. Each sample was stratigraphically located following previous studies (Ramos, 1970; Limarino *et al.*, 2001; Dávila & Astini, 2007; Nóbile *et al.*, 2008). For the Vinchina Basin, three samples every 5 cm were taken (in the same level) for Rb–Sr isotopic determinations, following the recommendations of Thomaz-Filho & Lima (1981). In the subsurface Bermejo Basin (San Juan province) two boreholes were sampled (cutting), the YPF.SJ.P.es-1 (Pozuelo, 5132 m) and Matagusanos E-1 (Matagusanos, 5996 mts) (Figs 3 and 4). Cutting material was collected every 200 m.

U–Pb dating

In order to constrain the maximum depositional ages, zircons extracted from three tuffaceous layers, two at the Quebrada de la Troya Norte and one at Quebrada de la Troya Sur, were analysed using the U–Pb LA-ICP-MS method. Zircons were separated from crushed rocks (3–5 kg) using conventional and heavy liquid and magnetic techniques. For each sample about 50–80 zircons were dated (see Appendix S1). Cathodoluminescence (CL) images of zircons were obtained using a Quanta 250 FEG electron microscope equipped with Mono CL3+ cathodoluminescence spectroscope (Centaurus) at the Geochronological Research Center in São Paulo University, Brazil. U–Pb analyses by LA-MC-ICP-MS were carried out using the Finnigan Neptune coupled to an excimer ArF laser (λ = 193 nm) ablation system also at the Geochronology Research Center of the São Paulo University. Ages were plotted using ISOPLOT 3.0 (Ludwig, 2003). Sample characterization included scanning electron microscope (SEM LEO 440I of the Institute of Geosciences – University of São Paulo, IGc/USP, with secondary electrons images and equipped with an Oxford Instruments micro-X-ray analyser) to produce textural images of grains of suitable size for micro-qualitative analysis.

XRD analyses on clay minerals

Separation of different clay minerals fractions (<2 μm; 2–1 μm, 1–0.2 μm, <0.2 μm, <0.1 μm, in more than 20 samples) was carried out following the recommendations of Moore & Reynolds (1997). The mineralogy of the different fractions was determined and semi-quantified through XRD analyses in oriented samples. For the clay minerals characterization (evolution of I/S with depth) of both the relationship between the content of illite and illite/smectite and the illite proportions in the I/S were established for all samples in each of the sections (see Appendix S1). In addition to XRD analysis, the different clay fractions (<2 μm, 2–1 μm, 1–0.2 μm, <0.2 μm and <0.1 μm) were evaluated using a laser particle analyser (Horiba LA-950).

TEM and chemical analyses

In order to complement and support the characterization of texture and composition of clay mineral phases at different levels, transmission electron microscope (TEM) analyses were performed on some samples using a Philips CM200 transmission electronic microscope. The textural analyses were carried out to detect the entire grain size spectrum. AES semi-quantitative analyses were carried out in approximately 20 grains per fraction using a scanning area of *ca*. 1000 × 200 Å (see Appendix S1). Chemical analyses using the metaborate/lithium tetraborate fusion procedure were done on approximately 0.1 g of each fraction. The major elements (including Rb, Sr and K) were analysed by ICP/OES (at Actlabs laboratories). Two fractions were separated: (1) those pretreated for removal of carbonates and organic matter (for K–Ar analyses) and those untreated (separated for Rb–Sr analyses).

Rb–Sr and K–Ar analyses

Rb–Sr and K–Ar isotopic analyses in separate fractions were performed at the Geochronological Research Center of IGc-USP (see Appendix S1). K–Ar ages were determined by PCM (Peak Comparison Method) in an ARGUS and a MAP-215-50 spectrometers. This method uses the ^{36}Ar atmospheric calibrator contained in a reservoir spectrometer, and allows calculating radiogenic ^{40}Ar in presence of until 99% of atmospheric ^{40}Ar (Gillot *et al.*, 2006) and detecting small amounts of radiogenic ^{40}Ar diluted by ^{40}Ar from atmospheric contamination.

I/S evolution modelling

Theoretical kinetics of smectite to illite transformation, for each of the studied sections, was based on the burial and thermal trajectories of Vinchina and Bermejo basins, previously established through the PetroMod 1D IES GmbH software (Collo *et al.*, 2011) constrained by the U–Pb zircon stratigraphic ages from the Vinchina Basin (Collo *et al.*, 2014, this work). The model proposed by Huang *et al.* (1993) was used to characterize the kinetics of transformation of smectite to illite (see Appendix S1 for more details).

(U–Th)/He ages

Six individual grains of apatite from two volcaniclastic samples were analysed by the U–Th/He method. Data were modelled to extract probable thermal histories using inverse modelling of the AHe ages with the HeFTy v1.8.0 software (Ketcham, 2005; Ketcham *et al.*, 2007). Wide model constraints based on the age of deposition, surface temperatures and AHe ages of individual grains, were used. Inverse models were run until 100 statistically good fit paths were achieved. If not possible, at least 100 acceptable paths were calculated. See Appendix S1 for more details on analytical procedures.

RESULTS

U–Pb dating

Figure 5 shows the U–Pb zircon ages (Appendix S2) obtained for the three tuff layers. For the stratigraphically lowest tuffaceous sample (TRT3 at *ca*. 5500 m depth), from the Quebrada de la Troya Norte, 78 grains were analysed and 60 yielded concordant ages (between 125% and 75%; Fig. 5a). Two main Tertiary (Andean) populations were detected at 12.62 ± 0.4 Ma (n = 3, 5%) and 20.84 ± 0.39 Ma (n = 4; 7%), with Th/U ratios between 0.30 and 2.2. Although this is the same tuffaceous level analysed by Dávila *et al.* (2008) and Collo *et al.* (2011), the population at 12.7 Ma had not been previously identified. For the uppermost tuff (TRT4 at *ca*. 750 m depth), 77 grains were analysed and 54 yielded concordant ages (between 160% and 85%; Fig. 5b). This sample has a unique Tertiary (Andean) population of 5.25 ± 0.23 Ma (n = 15, 28%) with Th/U ratios between 0.41 and 0.96. In both levels, the youngest ages were interpreted as good estimates of the sedimentation ages. The tuff from the bottom of section at the Quebrada de la Troya Sur (RLT4T2), produced 16 concordant ages (between 161% and 80%; out of 26 analyses). The youngest from a Tertiary (Andean) population of 16.3 ± 1.2 Ma (n = 7, 44%) (Th/U ratios between 0.3 and 0.7) is interpreted as the maximum sedimentation age. This age is comparable to that obtained by Ciccioli *et al.* (2014b) for the base of the Vinchina Formation at La Cueva section (15.6 ± 0.4 Ma). Moreover, the pool of ages supports reworking and high detrital contribution of the analysed tuffaceous samples. Other detrital populations present in the samples occur at 460 and 480 Ma (Ordovician) with minor peaks at 40–43, 225–341, 371–446, 493–542, 570–953 and 1013–1.155 Ma. These ages, present in all tuffaceous layers, show a noticeable age gap between the Late Triassic and

Palaeocene although this absence could be due to the low number of dated zircon grains.

Petrography and clay mineralogy

The bulk rock mineralogy of psammopelitic levels was established by X-ray diffraction and is summarized in the Appendix S3. The composition is similar to that determined by light and electron microscopy. Fine-grained white mica is the dominant phase among the mineral matrix assemblage, where quartz and plagioclase are also identified and a smaller amount of chlorite is also common. For samples from the Vinchina Basin sections (la Troya Norte and la Troya Sur), the potassium feldspar content is scarce. The content of this mineral is also variable in cutting samples from the Bermejo Basin. Most samples show weak diagenesis with only minor generation of argillaceous phases. There is an increase in flat contacts and corroded grains with increasing depth. From the SEM analyses, authigenic smectites are scarce (identified by their characteristic honeycomb-like morphology), and interstratified I/S and illite (neoformed?) are common in all samples. Among the matrix minerals detected by the SEM, the most abundant are: phengite, quartz and plagioclase. The abundant cement minerals observed under SEM are: analcime, heulandite and scarce smectite, interstratified I/S and iron minerals.

Clay mineral fraction from psammopelitic samples from the la Troya Norte section (Vinchina Basin) is mainly composed of illite, I/S, chlorite, quartz and plagioclase, with minor proportions of feldspar, haematite and zeolites (Fig. 6a; Table 1). The deepest samples show no K-feldspar that could be associated with the generation of I/S and illite. The K-feldspar, however, is present in the whole rock analysis, indicating that it was not completely broken down due to diagenetic processes.

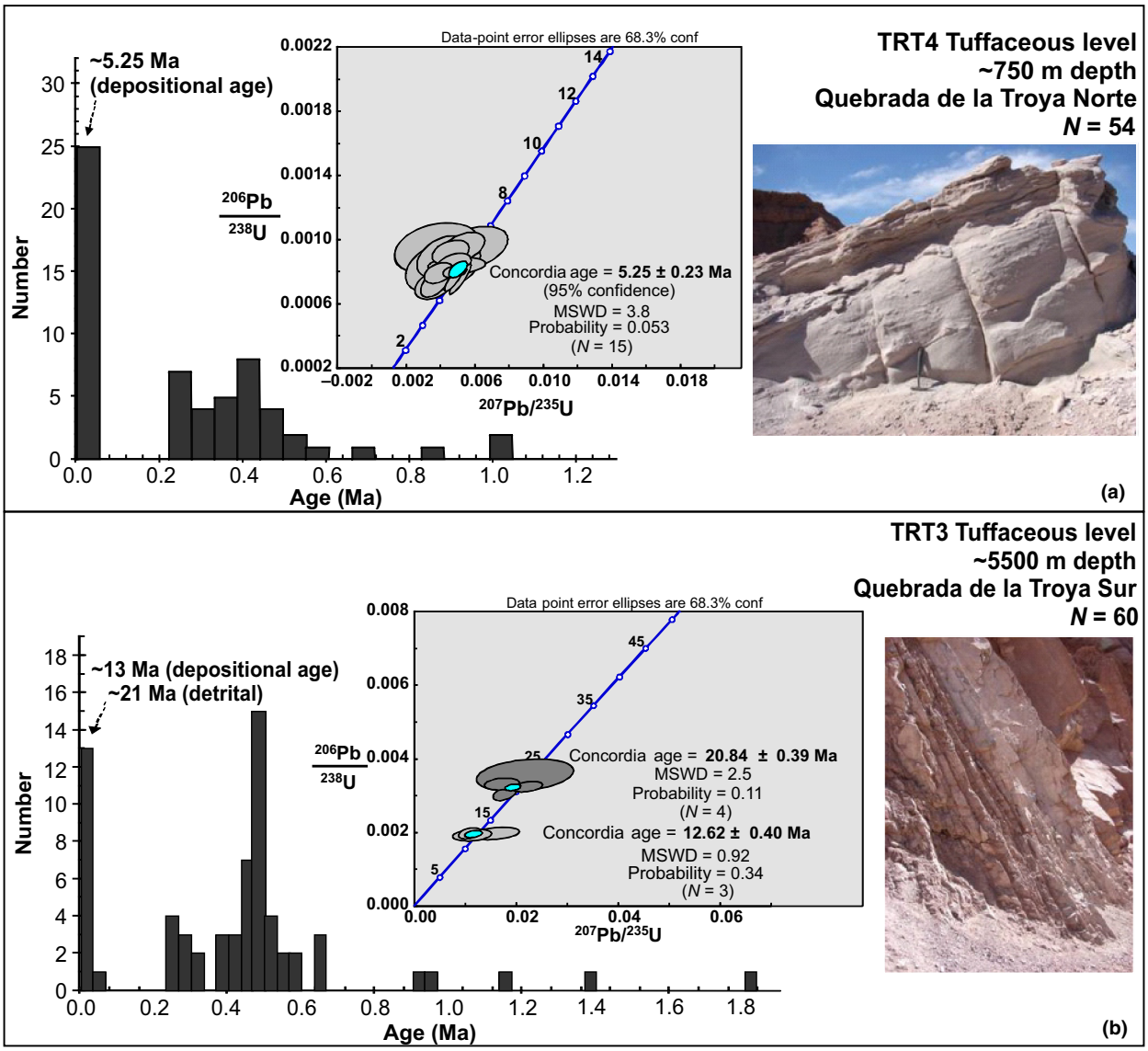

Fig. 5. Probability density plots showing the full range of zircon ages for tuffaceous levels within the Vinchina Basin. Concordia diagrams with interpreted depositional ages are also shown. (a) Toro Negro Formation; (b) Vinchina Formation.

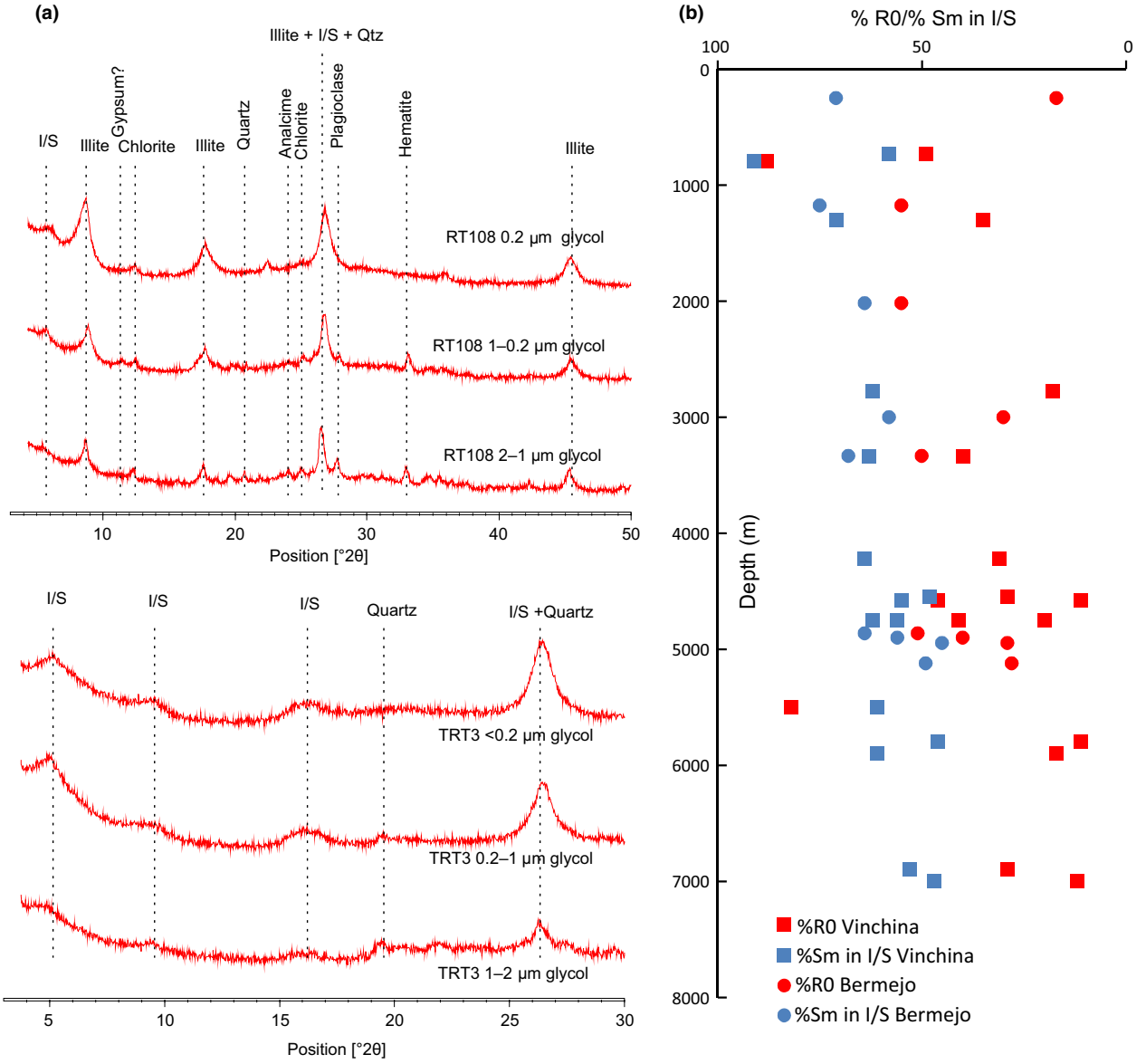

Fig. 6. (a) XRD diagrams on glycolated samples, (b) %R0/% smectite in I/S vs depth for both basins.

The volcaniclastic layers are mainly composed of interstratified I/S (Fig. 6a). Furthermore, in the fractions between 1 and 2 microns minor amounts of quartz and plagioclase were identified. In the la Troya Sur section (Vinchina Basin) the clay size fractions are mainly composed of illite, I/S and chlorite. Similar to the rocks of the la Troya Norte section, K-feldspar is present in the whole rock analysis, indicating that it was not totally consumed.

Clay single grains from one psammopelite and one tuffaceous (RT108 and TRT3, respectively) were analysed with TEM and SEM (Appendix S4; Figs 6b and 7). In RT108 structural formulas of the analysed grains are compatible with compositions ranging from interstratified I/S to illite, with interlaminar charges between 0.26 and 0.99 and Si contents between 3.09 and 3.99 a.p.f.u. Theoretical compositions of montmorillonite and illite (end members of the dioctahedral serie) indicate interlaminar charges of 0.27 and 0.8 respectively. According to that, the results point to the presence of interstratified I/S, with R0, R1, R3 ordering types, and illite in the four fractions. The relationship between interlaminar charges and the size of each grain are disclosed (see Fig. 6b). Grains are between the beidellite and montmorillonite aluminic fields. The tuffaceous sample fractions have silica contents that exceed 4 a.p.f.u., inconsistent with smectite, smectite/illite, illite or mica compositions. A tentative interpretation, supported by the texture of the analysed grains, is an uncompleted smectitization of the original volcanic glass, with Si, Ca and Na rich vitreous intercalations within the clay layers. This is also compatible with the higher Na and Ca contents and the S and Cl traces recorded in several grains of this tuffaceous level.

Table 2 shows the estimation of illite and I/S proportions, and smectite in the I/S contents obtained for each of the fractions analysed. Generally there is a continuous increase in illite content in I/S with depth. It should be

Table 1. Mineralogy present in oriented clay fractions aggregates of analysed levels. In bold are pointed levels separated for isotopic analysis

Clay mineral fraction composition (XRD)														
												Zeolites		
Depth (m)	Sample	Fraction	Illite	Clorite	I/S	Kaolinite	Gypsum	Quartz	Plagioclase	Feldspar	Haematite	Analcime	Heulandite	Sodalite
Vinchina Basin – La Troya Norte														
750	**RT100**	**<0.2 µm**		✓	✓									
		0.2–1 µm	✓	✓	✓			✓	✓	✓				
		1–2 µm	✓	✓	✓	¿?		✓	✓	¿?				
750	TRT4	<0.2 µm			✓									
		0.2–1 µm	✓		✓			✓	✓	✓				
		1–2 µm	✓		✓			✓	✓			✓		
1300	RT5	<2 µm	✓	✓	✓									
4550	**RT103**	<0.1 µm	✓		✓									
		<0.2 µm	✓	✓	✓									
		0.2–1 µm	✓	✓	✓			✓	✓		✓			¿?
		1–2 µm	✓	✓	✓			✓	✓	✓	✓	✓	¿?	¿? clinoptilolite?
	RT4		✓	✓	✓									
4750	RT3		✓	✓	✓									
5500	**TRT 3**	**<0.2 µm**			✓									
		0.2–1 µm			✓									
		1–2 µm			✓			¿?						
5800	**RT106**	**<0.2 µm**			✓									
		0.2–1 µm	¿?											
		1–2 µm	✓	✓	✓			✓	✓					
5900	RT2	<2 µm	✓	✓	✓									
6900	RT1	<2 µm	✓	✓	✓									
7000	**RT108**	**<0.1 µm**	✓		✓									
		<0.2 µm	✓	¿?	✓		¿?							
		0.2–1 µm	✓	✓	✓		¿?	¿?	✓		✓			
		1–2 µm	✓	✓	✓			✓	✓		✓	✓		
Vinchina Basin – La Troya Sur														
790	RLT11	<2 µm	✓	✓	✓									
2780	RLT8	<2 µm	✓	✓	✓									
3340	RLT7	<2 µm	✓	✓	✓									
4220	RLT6	<2 µm	✓	✓	✓									
4580	**RLT4**	**<0.2 µm**	✓	✓	✓						¿?			
		0.2–1 µm	✓	✓	✓				✓		✓		¿?	
		1–2 µm	✓	✓	¿?			✓	✓		✓		¿?	

(continued)

Table 1. (continued)

Clay mineral fraction composition (XRD)														
												Zeolites		
Depth (m)	Sample	Fraction	Illite	Clorite	I/S	Kaolinite	Gypsum	Quartz	Plagioclase	Feldspar	Haematite	Analcime	Heulandite	Sodalite
Bermejo Basin – Pozuelos														
250–255	SJP1	<2 μm	✓	¿?	✓	¿?		✓						
1175–1178	SJP2	<2 μm	✓	✓	✓			¿?	¿?					
2018–2022	SJP3	<2 μm	✓	✓	✓			✓	✓					
3000–3340	SJP4	<2 μm	✓	✓	✓			✓	✓				✓	
3336–3340	SJP5	<2 μm	✓	✓	✓			✓	✓				✓	
4900–4902	**SJ1**	**<0.2 μm**	✓	✓	✓				✓		¿?			
		0.2–1 μm	✓	✓	✓			✓	✓		✓	✓	¿?	¿?
		1–2 μm	✓	✓	✓	✓		✓	✓		✓	✓	¿?	¿?
4948–4952	**SJ2**	**<2 μm**	✓	✓	✓									
5122–5128	SJP6	<2 μm	✓	✓	✓									
Bermejo Basin – Matagusanos														
4865	**M1**	**<0.2 μm**	✓	✓	✓			✓	✓		✓		¿?	
		0.2–1 μm	✓	¿?	✓			✓	✓		✓	✓	¿?	¿?
		1–2 μm	¿?	✓	✓	✓		✓	✓		✓	✓	✓	¿?
4923–4926	**M2**	**<2 μm**	✓	✓	✓									

✓, present in the sample; ¿?, Dubious presence; I/S, interstratified illite/smectite.

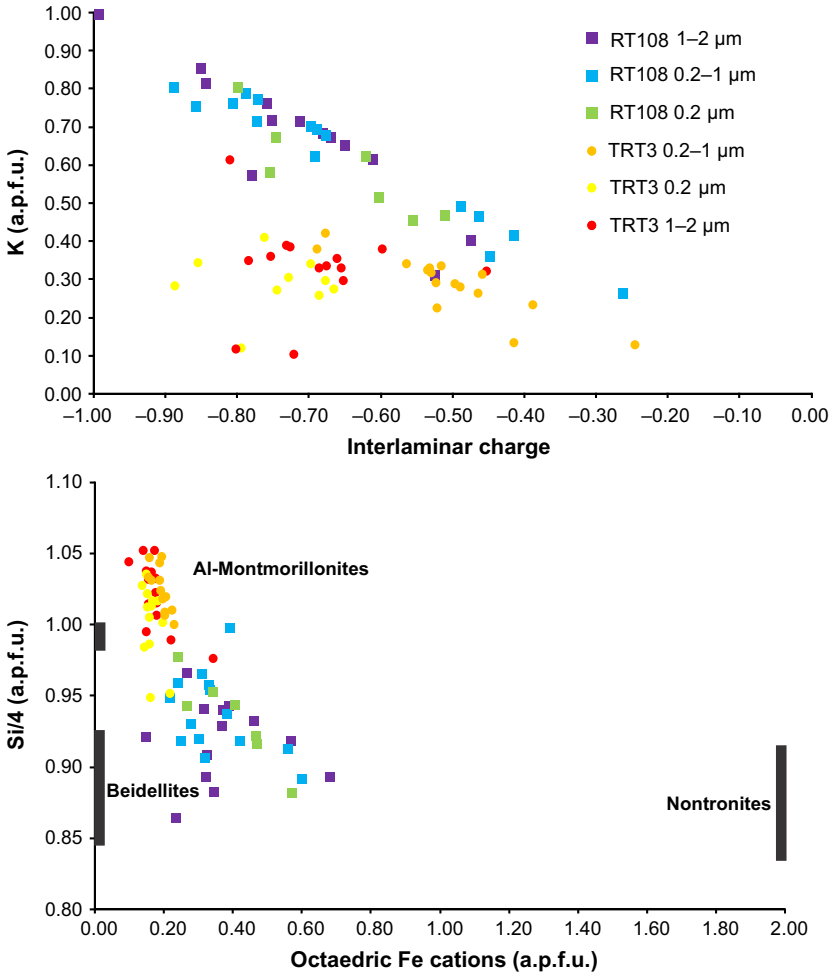

Fig. 7. SEM and TEM analyses on different clay mineral fraction from psammopelitic (RT108) and tuffaceous (TRT3) levels.

noted that many samples have a content >40% illite in the I/S. Środoń method (1981) shows illite values higher than those obtained by the decomposition of the XRD patterns, which allowed discriminating the presence of WCI, PCI and interstratified R3 ordering type. Table 2 shows the grain size distribution for each sample. Mean values are close to those of the fraction intended to be separated, and show that the procedure was more satisfactory in fine fractions. It is generally observed a normal type distribution, although some fractions showed two different populations.

Kinetic modelling of clay mineralogy

The kinetic modelling of the I/S evolution with depth in the Vinchina and Bermejo samples, considering different thermo-tectonic models of the basins (based on Collo *et al.*, 2011 and the modifications in sedimentation rates from Collo *et al.*, 2014, this work) is shown in Fig. 8. Distribution of measured I/S expandibilities for each sample is also shown.

Modelling with Petromod included the thermal flux conditions of *ca.* 300 ± 50 km from the trench, taking into account the crustal shortening. The thermal parameters for the normal subduction stage (30°C km^{-1}; 77.7 mW m^{-2}), the transitional stage (15°C km^{-1}, 38.85 W m^{-2}) and the flat subduction stage (10°C km^{-1}, 25.9 mW m^{-2}) were taken from Gutscher *et al.* (2000).

Vinchina Basin

For la Troya Note section the following sedimentation intervals were assumed: 16 to 12.6 Ma, 1500 m, 12.6 to 5.25 Ma, 4650 m; 5.25 to 3.40 Ma, 750 m. These sedimentation intervals are based on palaeomagnetic analysis and sedimentation rates established by Reynolds *et al.* (1990) and Re & Barredo (1993) and U–Pb zircon ages from Collo *et al.* (2011, 2014).

Model 1: Simulates the Neogene subduction dynamics in the Central Andes (Argentina) (cf. Yañez *et al.*, 2001), and includes the recovery for a normal subduction regime from 6 Ma to the present. *Model 2*: reproduces the Model 1 with a decrease in the geothermal gradient of *ca.* 25% following the isotherms model of Gutscher *et al.* (2000) for the continental crust. *Model 3*: reproduces the Model 1 but with an incomplete recovery of the geometry of the normal subduction regime, with a transitional scenario between the normal and flat subduction for the region between 8 and 3.4 Ma. *Model 4*: combines the conditions

Table 2. Illite and I/S proportions in the samples determined by the method proposed Środoń (1981) and proportions of illite in I/S determined by the Rettke (1980) and Lanson (1997) methods

			Środoń (1981)		Rettke (1980)	Lanson (1997)						
Depth	Sample	Fraction	%I/S	%illite	%smectite in I/S	WCI	PCI	% R3	% R1	% R0	Mean size*	Standard deviation*
Vinchina Basin – La Troya Norte												
750	RT100 (tuffaceous)	<0.2 μm										
	TRT4 (tuffaceous)	<0.2 μm										
		0.2–1 μm	90	10	68							
		1–2 μm	78	22	61							
	Toba2 (tuffaceous)											
	RT100 (psamopelite)	<0.2 μm	66	34	58	38		8	6	49		
		0.2–1 μm	0	100	46	54		11	17	18		
		1–2 μm	13	87	59	58		7	11	23		
1300	RT5 (psamopelite)				71	59		0	6	35		
1900	RT101 (psamopelite)											
3400	RT102 (psamopelite)											
4550	RT103	<0.1 μm				13	6	0	22	59	0.12935	0.0269
	(psamopelite)	<0.2 μm	21	79	48	28	23	13	8	29	0.18322	0.12
		0.2–1 μm	12	88	58	36	18	9	11	26	0.38034	0.7423
		1–2 μm	11	89	49	47	18	10	8	18	3.60225	0.4388
	RT4 (psamopelite)		20	80	56	63		10	6	20		
4750	RT3 (psamopelite)		29	71	62	43		11	5	41		
5400	RT104 (psamopelite)											
5500	TRT3	<0.2 μm	100		61	–	–	–	18	82		
	(tuffaceous)	0.2–1 μm	100		59	–	–	–	32	68		
		1–2 μm	100		46	–	–	–	33	67		
5800	RT106	<0.2 μm	0	100	46	59		22	8	11		
	(psamopelite)	0.2–1 μm	0	100		0		0	0	0		
		1–2 μm	27	86	58	37		31	12	20		
5900	RT2 (psamopelite)		21	89	61	69		10	4	17		
	RT1 (psamopelite)				53	43		24	5	29		
7000	RT108	<0.1 μm				13	6	0	22	59	0.13701	0.0262
	(psamopelite)	<0.2 μm	9	91	47	38	28	19	3	12	0.20991	0.2416
		0.2–1 μm	12	88	54	33	31	13	5	18	0.71426	0.6321
		1–2 μm	16	84	50	53	19	13	4	11	2.9761	0.9713
Vinchina Basin – La Troya Sur												
0	RLT13											
255	RLT12											
790	RLT11		82	18	91	12		0	0	88		
1408	RLT10											
1580	RLT9											
2780	RLT8		31	69	62	80		0	2	18		
3340	RLT7		18	82	63	38		15	7	40		
4220	RLT6				64	54		8	7	31		
4420	RLT5											
4580	RLT4	<0.2 μm	33	67	55	35	12	0	8	46	0.24013	0.26
		1–0.2 μm	17	83	56	37	14	0	16	33	0.509295	0.5947
		1–2 μm	21	79		37	10	13	17	23	2.859965	0.98785

(continued)

Table 2. (continued)

Depth	Sample	Fraction	Środoń (1981) %I/S	Środoń (1981) %illite	Rettke (1980) %smectite in I/S	Lanson (1997) WCI	Lanson (1997) PCI	Lanson (1997) % R3	Lanson (1997) % R1	Lanson (1997) % R0	Mean size*	Standard deviation*
4580	RLT3					76		8	5	11		
Bermejo Basin – Pozuelos												
250–255	SJP1		54	46	71	67		10	6	17		
1175–1178	SJP2				75	24		6	15	55		
2018–2022	SJP3		22	78	64	24		6	15	55		
3000–3340	SJP4		24	76	58	44		8	17	30		
3336–3340	SJP5		41	59	68	28		7	15	50		
4900–4902	SJ1	<0.2 μm	33	67	56	29	8	5	18	40	0.14904	0.26
		0.2–1 μm	27	73	59	24	13	8	6	50	0.63283	0.562
		1–2 μm		100	47	38	21	–	–	41	3.09472	1.0986
4948–4952	SJ2				45	50		12	10	29		
5122–5128	SJP6		25	75	49	49		13	10	28		
Bermejo Basin – Matagusanos												
4865	M1	<0.2 μm	29	71	64	27	6	0	16	51	0.21038	0.29
		0.2–1 μm	24	76	62	22	8	7	11	51	0.73087	0.7454
		1–2 μm	23	77		40	14	15	0	32	3.87428	0.4721
4923–4926	M2				46							
	SJM1											
	SJM2											

*Mean size and standard deviation of the grains present in each fraction are expressed in microns.

of the models 2 (decrease of *ca*. 25%) and 3. *Model 5*: reproduces the Model 2 but with an incomplete recovery of the geometry of the normal subduction regime, with a flat subduction regime for the region between 8 and 3.4 Ma. *Model 6*: considers the conditions of Model 4 in Bermejo Basin (see below).

Bermejo Basin

For the entire basin the following sedimentation intervals, based on sedimentary rates from Huaco section (Jordan *et al.*, 1993) were assumed: 14–10.3 Ma, 800 m, 10.3–8.4, 700 m, 8.4–6.7, 1100 m, 6.7–2.6, 2600 m, 2.6–2.3, 800 m.

Model 1: Considers the dynamics of Neogene subduction proposed by Yañez *et al.* (2001) and thermal parameters calculated by Gutscher *et al.* (2000) for different subduction contexts. Importantly, no significant differences in terms of heat flow were observed between this model and the proposal by Ramos *et al.* (2002) for the regional development. Model 2: considers an increase of about 30% in the thermal parameters Gutscher *et al.* (2000). This increase was considered as temperatures obtained in Model 1 are not enough to reach current maximum temperatures recorded from analyses of well logging in the region (see Fig. 8).

Model 3: Considers that the current thermal gradient (*ca*. 20°C km^{-1}) existed in this sector of the basin since 9 Ma (model proposed by Ramos *et al.*, 2002). Model 4: Considers a heat flow of 42 mW m^{-2} from 9 Ma in order to obtain an adjustment to final temperatures recorded in the borehole data.

Clay geochronology

Rb–Sr dating

Table 3 summarizes the Rb–Sr results. The $^{87}Rb/^{86}Sr$ versus $^{87}Sr/^{86}Sr$ diagram shows a linear relationship between residue and untreated aliquots from <2 μm fractions whereas the leachates present variable disturbance ($^{87}Sr/^{86}Sr$ between 0.70693 and 0.740270; Fig. 9). Isochrones in this psammopelites (<2 μm fractions) show ages between 125 and 165 Ma, except for M2 sample (Matagusanos) that yields an age of 234 Ma. For RT106 sample (psammopelite), the $^{87}Rb/^{86}Sr$–$^{87}Sr/^{86}Sr$ diagrams (leachate, residue and untreated alicuots for each fraction) show good alignment, and produce three linear arrays: *ca*. 176 ± 6 Ma (bulk rock, initial $^{87}Sr/^{86}Sr$: 0.70927 ± 0.00039, MSWD: 1.7), 167 ± 57 Ma (0.2–1 μm fraction, initial $^{87}Sr/^{86}Sr$: 0.7079 ± 0.0078, MSWD: 3) and *ca*. 100 ± 7 Ma (<0.2 μm fraction, initial $^{87}Sr/^{86}Sr$: 0.7082 ± 0.0020). The tuffaceous level TRT3 (<0.2 and 0.2–1 μm fractions) depicted an isochron of 6 ± 1.4 Ma (initial $^{87}Sr/^{86}Sr$: 0.70836 ± 0.00031, MSWD: 1185?), whereas the coarser fraction yielded a significantly older isochron of 29 ± 0.35 Ma (initial $^{87}Sr/^{86}Sr$: 0.70834 ± 0.00001).

K–Ar dating

Table 4 presents the K–Ar ages for the different fractions for each sample. The younger K–Ar ages of the pelitic levels correspond to finer fractions (Fig. 10, 136–224 Ma, for 1–2 μm; 112–159 Ma, for 0.2–1 μm; 76–116 Ma, for

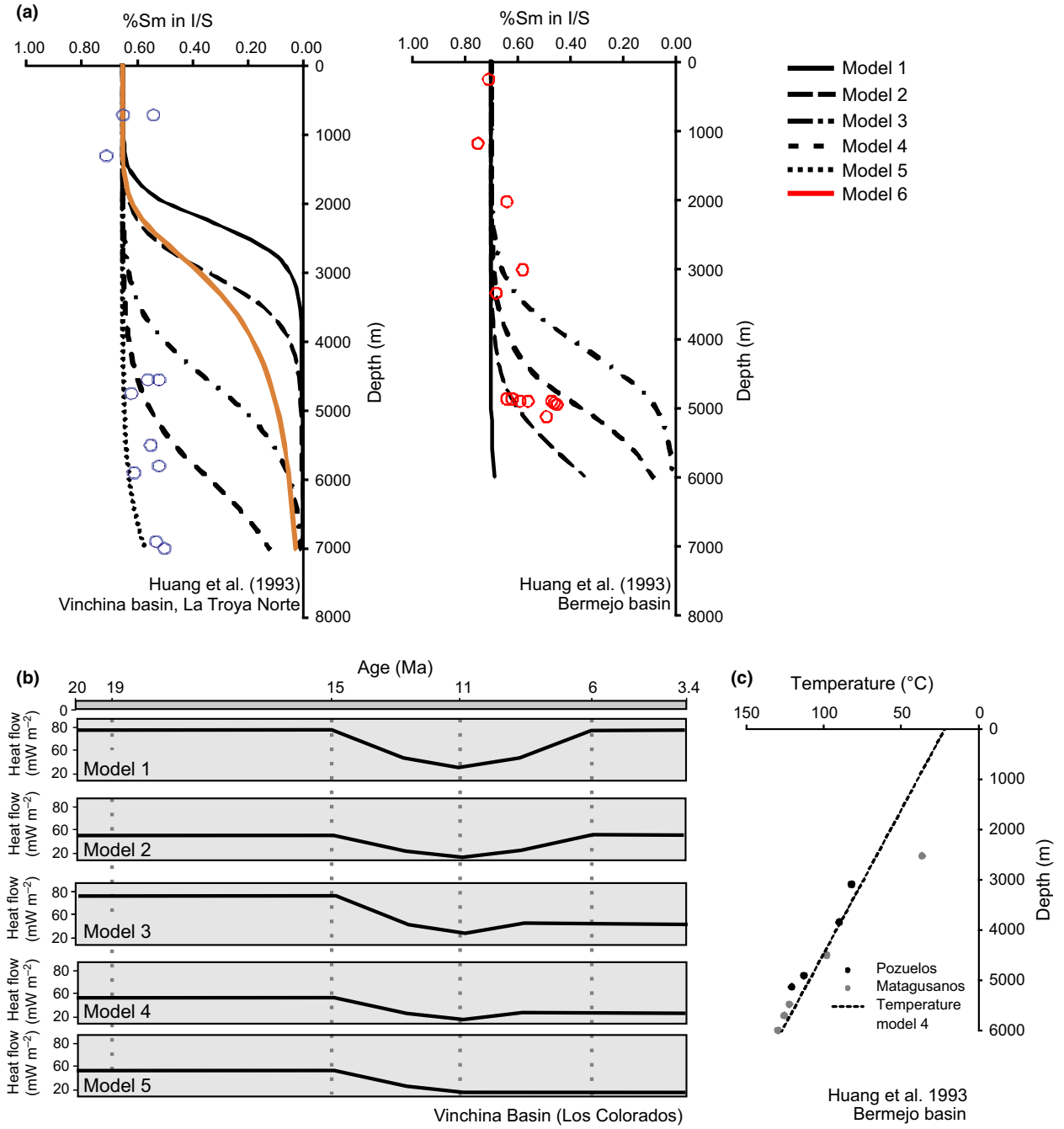

Fig. 8. (a) Kinetic models of the I/S evolution with depth in the two basins, circles show values from analysed samples. (b) Heat flow trajectories for each of the five models in the Vinchina Basin (la Troya Norte section). (c) Borehole temperatures for the Bermejo Basin (Pozuelos and Matagusanos) and theoretical temperature with depth from model 4. In both basins: continental with PWD zero and SWIT = *ca.* 0°C. The thermal conductivity used for transforming thermal gradients at values to heat flux was: 2.59 (W mK^{-1}) (from the software). In A, the red line shows the trajectory considering the thermal conditions for model 4 in Bermejo Basin.

<0.2 μm and 39.3–42 Ma, for <0.1 μm). Atmospheric ^{40}Ar ranges between 2.7 to 16.6 and 24.1% to 63%. In the tuffaceous level, the same relation between grain size and age is observed, but obtained ages are substantially younger than those in psammopelitic levels (21.3–12 Ma). Atmospheric ^{40}Ar concentrations are much greater than those from psammopelites (27%, 30% and 85%). Ages for the same clay fraction show a similar bracket, with a slight decrement of the values with depth (Fig. 10). In addition to clay fractions, biotite grains separated from the tuffaceous level TRT4 (top of the Vinchina Fm. at la Troya Norte section) were dated by this method supplying an age of 6.4 ± 0.5 Ma.

Apatite (U–Th)/He (AHe) thermochronology

Tables 5 and 6 present the He results for two tuffaceous samples from the bottom sections in Vinchina Basin. The

Table 3. Analytical Rb–Sr data in the analysed fractions (L, leached fraction; R, residue)

									Isochron	
Sample	Aliquot	Depth	Rb (ppm)	Sr (ppm)	Rb^{87}/Sr^{86}	Error	Sr^{87}/Sr^{86}	Error	Age (Ma)	Error
Vinchina Basin – La Troya Norte										
RT100	Psamopelite <0.2 μm – U	750	125.20	55.0	6.6030	0.1030	0.71829	0.000037	111	2
	L		0.70	27.0	0.0751	0.0012	0.70818	0.000100		
	R		160.79	38.2	12.2108	0.1013	0.72741	0.000140		
RT103a	Psamopelite <2 μm – U	4550	170.87	166.2	2.9778	0.0239	0.71334	0.00006	130	51
	L		0.36	28.5	0.0367	0.0006	0.70777	0.00009		
	R		191.03	148.4	3.7279	0.0420	0.71450	0.00005		
RT103b	Psamopelite <2 μm – U		181.44	167.7	3.1333	0.0252	0.71381	0.00007	133	5
	L		0.39	30.2	0.0370	0.0007	0.70803	0.00010		
	R		193.22	152.7	3.6655	0.0411	0.71494	0.00006		
RT103c	Psamopelite <2 μm – U		181.92	163.3	3.2259	0.0262	0.71478	0.00005	153	7
	L		0.34	34.5	0.0289	0.0005	0.70783	0.00017		
	R		197.73	138.8	4.1278	0.0457	0.71674	0.00007		
TRT3	Tuffaceous <0.2 μm – U	5500	118.31	338.0	1.0129	0.0081	0.70845	0.00007	6	1.4
	L		83.80	247.3	0.9810	0.0079	0.70834	0.00005		
	R		162.28	165.0	2.8470	0.0499	0.70861	0.00005		
	Tuffaceous 0.2–1 μm – U		128.00	1321.0	–	–	0.70855	0.00005	29	0.35
	L		0.98	195.6	0.0144	0.0002	0.70837	0.00003		
	R		135.92	529.1	0.7436	1.0102	0.70841	0.00003		
	Tuffaceous 1–2 μm – U		117.00	1256.0	0.0830	0.0007	0.70826	0.00005		
	L		0.80	237.3	0.0097	0.0002	0.70834	0.00007		
	R		66.84	796.1	0.2430	1.0125	0.70844	0.00005		
RT-106	Bulk rock/Psamopelite – U	5800	193.80	180.5	3.1110	0.0320	0.71705	0.000051	176	6
	L		1.49	50.7	0.0857	0.0839	0.71057	0.000820		
	R		186.26	75.7	7.1323	0.0567	0.72718	0.000070		
	Psamopelite <0.2 μm – U		229.90	60.0	11.1130	0.3300	0.72393	0.000029	100	7
	L									
	R		280.37	38.4	21.2204	0.1742	0.73825	0.00009		
	Psamopelite 0.2–1 μm – U		237.10	63.1	10.9090	0.2120	0.73311	0.000046	167	57
	L		0.45	12.4	0.1060	0.0025	0.70824	0.000110		
	R		235.66	50.7	13.5012	0.1095	0.74027	0.000060		
RT108a	Psamopelite <2 μm – U	7000	197.95	119.9	4.7839	0.0380	0.71841	0.00009	159	4
	L		0.53	46.5	0.0327	0.0022	0.70766	0.00014		
	R		207.55	78.7	7.6487	0.0660	0.72487	0.00007		
RT108b	Psamopelite <2 μm – U		193.25	155.1	3.6100	0.0291	0.71607	0.00007	165	7
	L		0.53	70.2	0.0218	0.0075	0.70729	0.00041		
	R		200.01	89.9	6.4476	0.0575	0.72265	0.00007		
RT108c	Psamopelite <2 μm – U								165	6
	L		0.43	71.1	0.0174	0.0030	0.70750	0.00027		
	R		197.85	82.4	6.9620	0.0609	0.72379	0.00006		
Vinchina Basin – La Troya Sur										
RLT4a	Psamopelite <2 μm – U	4580	196.90	211.9	2.6904	0.0213	0.71377	0.00005	125	9
	L		0.40	46.4	0.0251	0.0007	0.70919	0.00020		
	R		213.82	169.0	3.6650	0.0357	0.71565	0.00010		
RLT4b	Psamopelite <2 μm – U		197.71	208.1	2.7514	0.0222	0.71381	0.00006	141	7
	L		0.44	46.6	0.0272	0.0017	0.70832	0.00015		
	R		208.15	161.7	3.7282	0.0382	0.71572	0.00005		
RLT4c	Psamopelite <2 μm – U		173.97	216.0	2.3319	0.0188	0.71274	0.00007	131	55
	L		0.43	62.8	0.0196	0.0002	0.70828	0.00010		
	R		209.58	176.5	3.4392	0.0394	0.71461	0.00005		
Bermejo Basin – Matagusanos										
M2	Psamopelite <2 μm – U	4923–4926	142.20	695.1	0.5922	0.0048	0.70957	0.00009	234	18
	L		1.66	–	–	–	0.70891	0.00009		
	R		168.41	241.4	2.0209	0.0442	0.71433	0.00007		

(continued)

Table 3. (continued)

Sample	Aliquot	Depth	Rb (ppm)	Sr (ppm)	Rb^{87}/Sr^{86}	Error	Sr^{87}/Sr^{86}	Error	Isochron Age (Ma)	Isochron Error
Bermejo Basin – Pozuelos										
SJ2	Psamopelite <2 μm – U	4948–4952	133.45	887.1	0.4357	0.0035	0.70919	0.00006	153	560
	L		0.70	42.5	0.0478	0.0023	0.70693	0.00034		
	R		176.44	234.3	2.1809	0.0315	0.71210	0.00009		

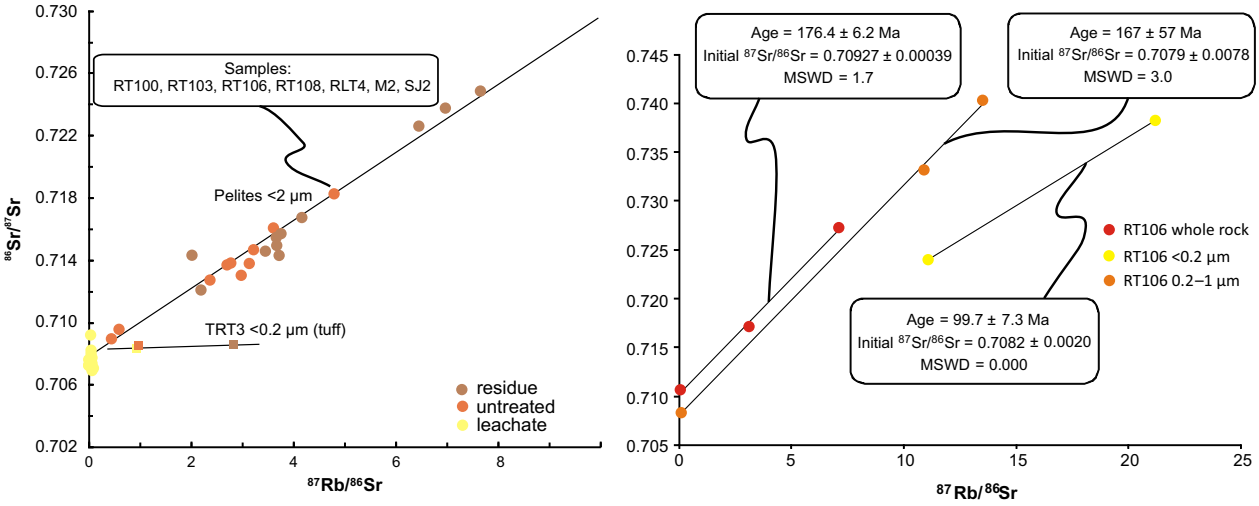

Fig. 9. Distribution of Rb–Sr ages. U: untreated (orange), L: leachate (yellow), R: residue (brown).

corrected AHe ages yielded ages from 3.3 Ma to 7.4 Ma. These ages are younger than the U–Pb depositional ages suggesting a post-depositional resetting (temperatures between 40°C and 80°C, Wolf *et al.*, 1998, Stockli *et al.*, 2003), likely due to burial. Mean ages are similar for both samples with values of 5.8 ± 0.7 (TRT3) and 5–6 ± 0.7 (RLT4T2). A positive but nonlinear correlation between (U–Th)/He date and eU is observed. Modelling results are illustrated in Fig. 11 (one grain of the TRT3 in Fig. 11a and two grains of the RLT4T2 in Fig. 11b). For TRT3 the weighted mean path shows maximum temperatures of *ca.* 75°C at *ca.* 4.75 Ma while best-fit model shows maximum temperatures of *ca.* 58°C at *ca.* 0.5 Ma, just before the beginning of exhumation. For RLT4T2, mean path maximum temperatures of *ca.* 83°C between *ca.* 7 and 6 Ma and the best-fit model provides maximum temperatures of *ca.* 73°C at *ca.* 2.8 Ma.

DISCUSSION

Geocrhonologic and thermochronologic interpretations

Considering that sedimentation in the Vinchina and Bermejo basins started at approximately 16 and 20 Ma, respectively (U–Pb data, Ciccioli *et al.*, 2014b; sample RLT4T2 this work; Jordan *et al.*, 2001), the Rb–Sr isochron ages might reflect a mixture of diagenetic and detrital material. Sample RT106 shows younger ages with decreasing particle size in agreement with the presence of a greater proportion of diagenetic material, as suggested by the XRD analysis and the mineral chemistry of the material. The recurrence of ages *ca.* 150 Ma might indicate the signature of a relatively homogeneous source area for both the Vinchina and Bermejo basins during the Neogene. Moreover, the outcrops currently exposed near these basins have different ages (see Pastillos and Fiambialá geological maps) and provenance analysis show variable contribution from the Western Sierras Pampeanas (Toro Negro and Umango Ranges), Cordillera Frontal and Precordillera from Miocene to early Pliocene (Ciccioli *et al.*, 2014b). The $^{87}Sr/^{86}Sr$ ratios for leachate are between 0.70693 and 0.710570, and likely reflect a mixture of detrital signatures from a heterogeneous source area or the influence of isotopic characteristics of the continental depositional environment of the studied sequences. This heterogeneity is also revealed by the broad distribution of detrital zircon ages of the tuffaceous and psammitic levels of la Troya Norte and la Troya Sur sections (Vinchina Basin, Collo *et al.*, 2014, this work). The isochron age of the psammopelite M2 (in Matagusanos, see location in Fig. 3) is *ca.* 100 Ma older than the rest of the samples, which could be interpreted as a different source area supply during the Miocene in this region.

The K–Ar ages show similar patterns to the Rb–Sr data, i.e. ages older than onset of sedimentation. This is

Table 4. Analytical K–Ar data in the analysed fractions

Sample	Material	% K~error	$^{36}Ar/^{38}Ar$	Error	^{40}Ar Atm (%)	Error	Age (Ma)	Error
Vinchina Basin – La Troya Norte								
TRT4	Biotite	8.00~0.01	3.4	0.6	57	3	6.4	0.5
RT100 1–2	Psamopelite	3.59~0.01	7	0.4	5.7	0.2	174	2
RT100 0.2–1	Psamopelite	3.58~0.01	7.6	0.6	8	0.2	154	2
RT100 0.2	Psamopelite	2.05~0.01	5.4	0.1	63	1	103	5
RT103 1–2	Psamopelite	3.95~0.01	6.1	0.5	4.3	0.2	181	3
RT103 0.2–1	Psamopelite	4.26~0.01	6.3	0.3	6	0.1	146	2
RT103 0.2	Psamopelite	3.98~0.01	6.1	0.2	16.6	0.4	76	1
RT103 0.1	Psamopelite	3.98~0.01	5.7	0.1	39.7	0.4	39,3	0,6
TRT3 1–2	Tuffaceous level	2.20~0.01	8	1	26.7	0.7	21.3	0.4
TRT3 0.2–1	Tuffaceous level	2.30~0.01	2.48	0.07	30	1	17	0.6
TRT3 0.2	Tuffaceous level	1.63~0.01	5.2	0.1	85	1	12	0.5
RT108 1–2	Psamopelite	4.34~0.01	5.6	0.3	2.7	0.2	136	2
RT108 0.2–1	Psamopelite	4.77~0.01	6	0.3	3.4	0.1	112	2
RT108 0.2	Psamopelite	4.87~0.01	8.2	0.4	5.6	0.3	79	2
RT108 0.1	Psamopelite	4.90~0.01	5.1	0.2	24.1	0.3	42	0.4
Vinchina Basin – La Troya Sur								
RLT4 1–2	Psamopelite	3.30~0.01	6.2	0.5	6	0.2	163	2
RLT4 0.2–1	Psamopelite	3.79~0.01	5.4	0.2	7.4	0.1	144	2
RLT4 0.2	Psamopelite	3.13~0.01	5.7	0.2	15.3	0.3	90	1
Bermejo Basin – Matagusanos								
M1 1–2	Psamopelite	2.61~0.01	6.1	0.6	4	0.1	224	3
M1 0.2–1	Psamopelite	3.05~0.01	4.9	0.2	4.7	0.1	159	2
M1 0.2	Psamopelite	3.07~0.01	5.3	0.2	10.2	0.2	116	2
Bermejo Basin – Pozuelos								
SJ1 1–2	Psamopelite	2.38~0.01	67	60	6.6	0.2	151	2
SJ1 0.2–1	Psamopelite	2.81~0.01	5.2	0.1	12.3	0.3	138	2
SJ1 0.2	Psamopelite	3.11~0.01	5.34	0.06	35	0.6	82	1

similar to the Rb–Sr data for the RT106 sample, which reinforces the idea of a higher contribution of detrital components for the coarser fractions. The K–Ar ages of the tuffaceous bed (TRT3) are consistent with a lower contribution of detrital material, whereas the fine fraction might be associated with a timing of diagenesis (Fig. 10a).

The relationship between the obtained ages and the relative (Środoń, 1999) or absolute (Pevear, 1992) concentrations of detrital and authigenic components (Table 4) can be used to calculate the mixed ages. A possibility is that all of the I/S is representative of the diagenetic component and that illite ratios represent the detrital component (Pevear, 1999; Van der Pluijm & Haines, 2008; among others). The method of Lanson (1997), considering the R1, R3 and illite set as detrital and R0 as the diagenetic phase, demonstrates a good correlation. However, any reasonable diagenetic ages could be estimated from the regression curves for each sample (Fig. 10b).

Also noteworthy is that there is a K–Ar correlation between the age's rejuvenation and depth of the sample (Fig. 10a). Sample RT108 (from 7000-m depth, near the bottom) shows the youngest ages and the smaller proportion of R0 (12%) in the <0.2 fraction (<0.2). In both basins, the main neoformed mineral contribution to the K–Ar dating is from the bottom sections, i.e. the major depths (see Fig. 10). The differences in ages between shallow and deeper levels, as well as between different grain sizes might be interpreted as related to the process of clay mineral growth. If the time required for the formation of a mineral is short, the closure would be instantaneous. In this case, the average measured age would be the age of the mineral growth and ages corresponding to different grain sizes in a given sample would be comparable. If the mineral continues growing for a long time, the closure is long, the age would be an "integrated age" or "mixed age", whose value would depend on the duration of the growth. In this case, the ages obtained from different grain sizes fractions would tend to be different. In general, the burial of sedimentary sequences is a long term process, ranging from a few million to tens of millions of years, and the obtained ages should be treated as mixed ages. Consequently, a suitable explanation might relate the distribution of age with grain size of the analysed illites (Środoń *et al.*, 2002). In the case of the Vinchina and Bermejo basins, long-lived growth mechanisms, with higher contents of neoformed clays, developed during the long basin subsidence and burial with a progressive illitization process.

The best-fit as well as weighted mean temperature–time paths from AHe data, yellow and black lines in Fig. 11, are consistent with the subsidence history deduced from sedimentation rate studies, constrained with U–Pb ages (Ciccioli *et al.*, 2014b; Collo *et al.*, 2014) and magnetostratigraphy (Reynolds *et al.*, 1990; Re &

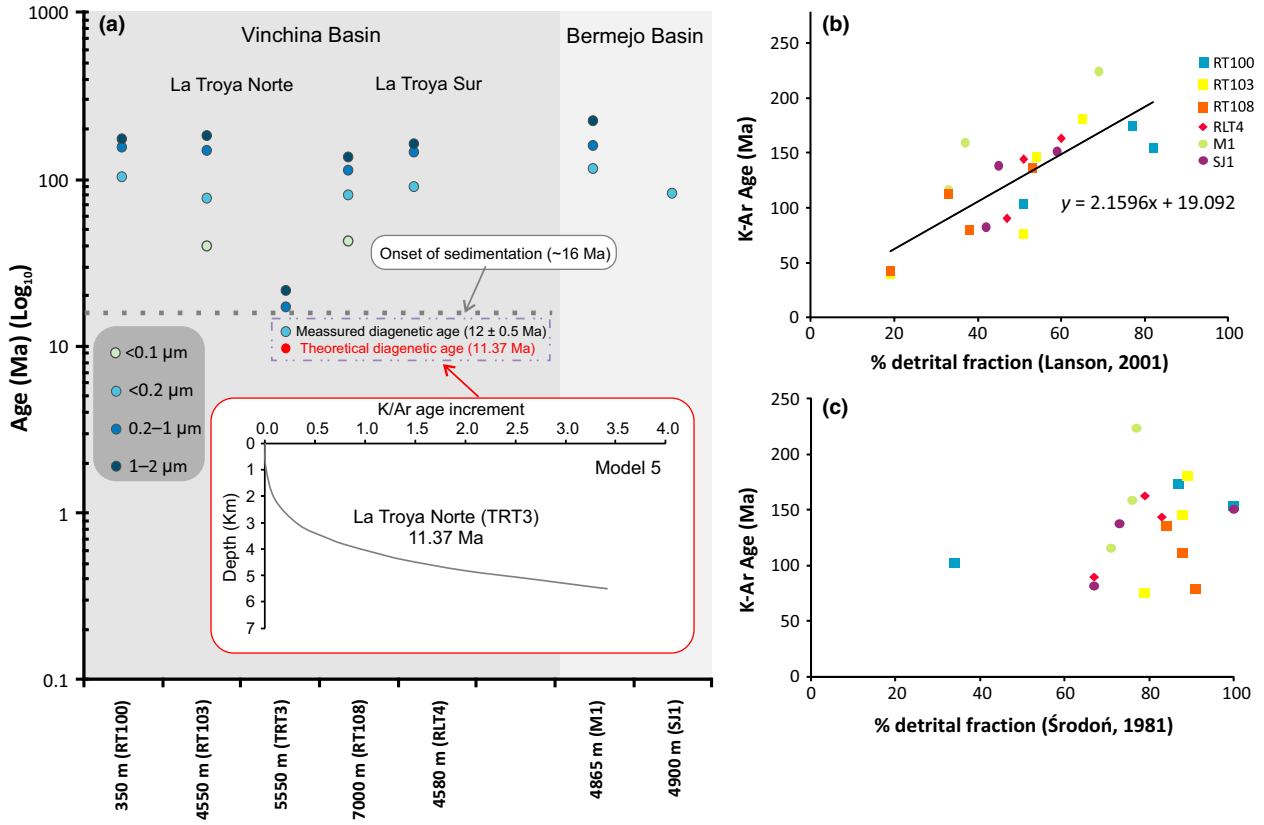

Fig. 10. (a) Distribution of the K–Ar ages; the theoretical K–Ar age for the TRT3 level is detailed. (b) Relation between % detrital fraction (determined through the Lanson, 1997 decomposition proposal) and obtained ages. See that the regression curve intersects the y axis at *ca*. 19 Ma, which is similar to the age for the onset of the sedimentation. (c) Relation between % detrital fraction (from Środoń, 1981 proposal) and obtained ages. The distribution does not show a coherent pattern.

Table 5. Apatite (U–Th)/He data

Sample	4He (ncc)	Mass (mg)	U (ppm)	Th (ppm)	Th/U ratio	Width (µm)	Grain length (µm)	Raw Age (Ma)	FT	Corrected Age (Ma)	Error (±1σ)	Weighted mean age	±2 sigma	eU
TRT3														
1	0.0088	0.0011	22.7	28.9	1.28	98	78	2.2	0.67	3.4	0.2	5.8	0.7	29.5
2	0.0189	0.0006	52.4	38.3	0.73	78	68	3.9	0.61	6.9	0.4			61.4
RLT4														
1	0.0417	0.0015	24.3	174.8	7.20	120	75	3.4	0.70	5.1	0.3	**5.6**	**0.7**	65.4
2	0.0270	0.0006	28.0	249.1	8.90	90	54	4.1	0.60	7.4	0.5			86.5
3	0.0223	0.0007	37.2	259.5	6.98	89	60	2.7	0.61	4.8	0.3			98.1
4	0.0097	0.0005	38.3	243.3	6.35	80	53	1.7	0.57	3.3	0.2			95.5

Table 6. HeFTy modelling constraints

Sample	Depositional Age (Ma)	Depositional temperature °C	Burial Age (Ma)	Burial temperature °C	Present temperature °C	Grains Modelled	Total paths	Acceptable paths	Good paths
TRT3	12.7	20	5.5–0	20–150	20	1	4887	173	100
RLT4T2	16.3	20	9.2–0	20–150	20	3, 4	1184	118	100

Barredo, 1993). This curves show a long residence time (between 5 and 10 Ma) within the AHePRZ (Apatite Helium Partial Reseating Zone) zone, with maximum temperatures below 80°C. After this residence rapid exhumation would occur between approximately 4 and 0.5 Ma. This is consistent with the deformation of the

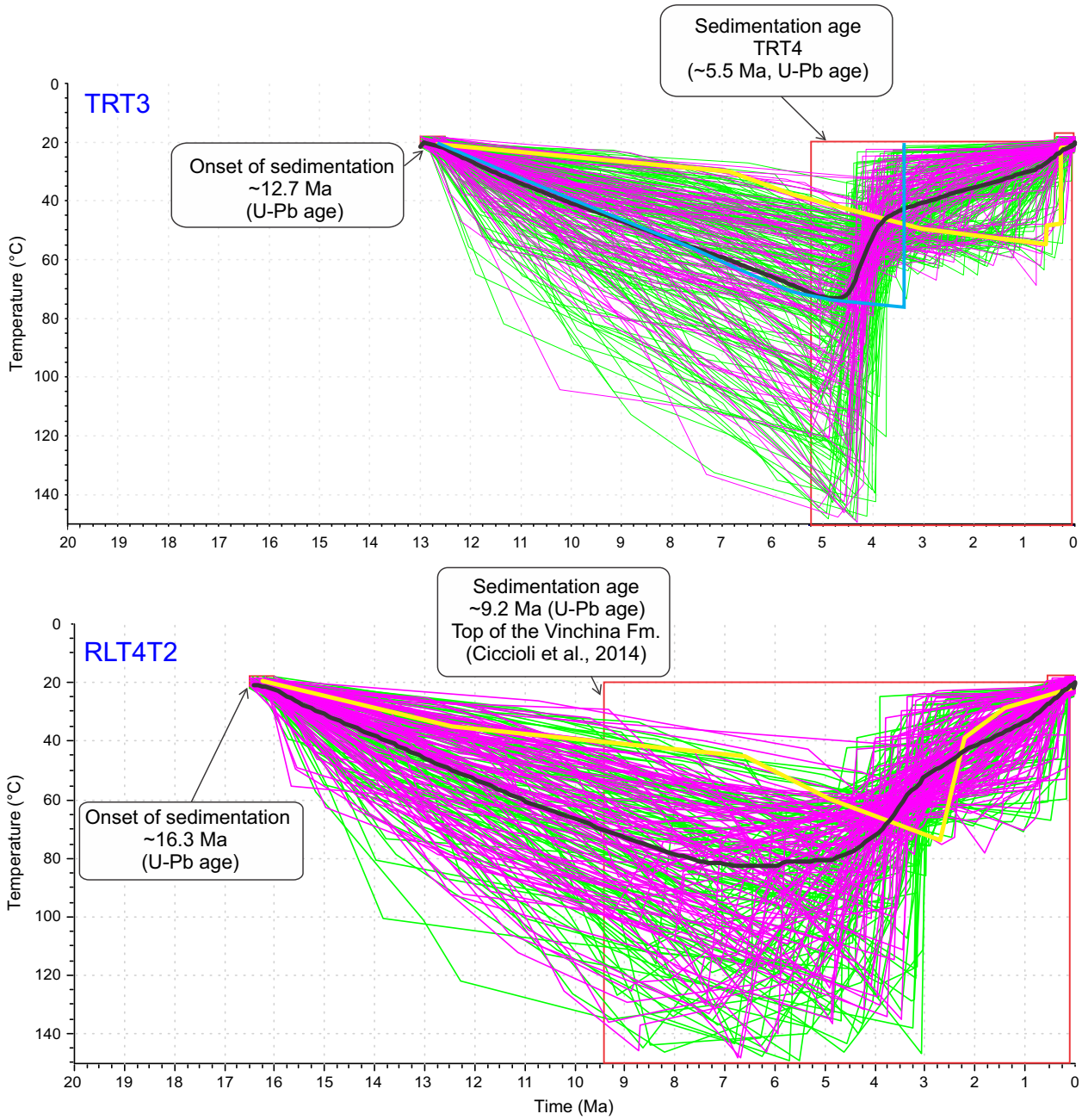

Fig. 11. (U–Th)/He ages modelling with HeFTy. Yellow lines: Best-fit models; black lines: Mean models; light blue line: Model for TRT3 from Petromod; red rectangles: Age–temperature constraints. In green acceptable paths, in purple good paths.

Mio-Pliocene Vinchina and Bermejo basins topped by Plio-Pleistocene? conglomerates (see previous section). This also correlates with AHe ages and eU. According to Flowers *et al.* (2009), the RDAAM model predicts a positive correlation for peak heating temperatures between 30°C and 100°C as well as for prolonged residence in the AHePRZ. Temperatures are also consistent with estimations from clay mineralogy and isotopic analyses (see light blue line in Fig. 11). Figure 11a also illustrates the trajectory modelled with Petromod considering the sedimentation rate, erosion gaps, changes in the heat flow and mineralogy, which is also strongly similar to the weighted mean model estimated from thermochronology (HeFTy). However, it should be noted that the apatite He modelling results, with the available constraints, are also compatible with higher temperature burial histories (*ca.* 140°C) compared to the clay mineralogy (R0 ordering is not stable at *ca.* 120°C) and the AFT data (Coughlin, 2002).

Thermal history of Vinchina and Bermejo basins

The transformation of clay minerals along the alluvial succession shows a distribution of I/S phases (in both

sedimentary basins) that defines a progressive illitization (R0 → R1 → R3 → I) related to the burial history of the succession and associated with an increase of ordering in the I/S and illite content from the top to bottom (Nóbile *et al.*, 2008; Collo *et al.*, 2009, 2011). The degree of illitization and stratigraphic position show a strong correlation. The presence of R0 even in deeper levels (stratigraphically the lowest strata) demonstrate that the base of both basins would have not exceeded the diagenetic field (*ca*. 120°C cf. Frey & Robinson, 1999). If we compare the I/S interstratified distribution in the Vinchina Basin with simulated data, a heat flow of *ca*. 26 mW m^{-2} results for the flat subduction regime between 8 and 3.4 Ma (model 5 in Fig. 8). This model, which takes into account the new sedimentation rate of *ca*. 0.6 mm yr^{-1} that characterize the basin fill between *ca*. 13 and 5 Ma, agrees with the maximum temperatures reported by Collo *et al.* (2011) and the lack of Neogene exhumation ages showed by Dávila & Carter (2013). In the Bermejo Basin, the distribution of interstratified I/S is compatible with a model that considers a heat flow of 42 mW m^{-2} since 9 Ma, with final temperatures similar to those observed in boreholes (model 4 in Fig. 8). Also, the heat flow values are comparable to those obtained for the same basin from magnetotelluric analysis (36–40 mW m^{-2}; Borzotta *et al.*, 2009) and agree with heat flow calculations reported by Hamza *et al.* (2005) along the modern Andean foreland. The results for the Vinchina Basin, located today on the transitional segment between normal and flat slab subduction, reinforce the interpretation of a flat subduction thermal regime, i.e. extremely cold, which would have not yet adjusted to a normal subduction regime during the Pliocene, i.e. to hotter situations (Collo *et al.*, 2011). For the Bermejo Basin, the thermal state estimated for the Neogene-present interval is consistent with a low heat flow, but higher than that proposed by Gutscher *et al.* (2000). It is important to notice that, for the Bermejo model, the sedimentation intervals were taken from studies on the exhumed Huaco section (Johnson *et al.*, 1986; Jordan *et al.*, 1993, 2001).

The absolute ages (Rb–Sr and K–Ar) obtained for the psammopelitic levels are older than the sedimentation ages of the basins and, consequently, do not constrain the thermal modelling. However, the high amount of detrital grains even in the finest fractions at the deepest levels, suggest a weak diagenesis and extremely low thermal flux history for the region. This reinforces the idea of cold foreland basins proposed by Collo *et al.* (2011), and corroborated by others (Dávila & Carter, 2013; Richardson *et al.*, 2013; Bense *et al.*, 2014; Hoke *et al.*, 2014). Considering a deposition age of *ca*. 13 Ma for the TRT3 level (U–Pb detrital zircons), the K–Ar ages of the tuffaceous level show a detrital contribution, although in a lower proportion. Hence, the K–Ar ages for the two coarsest fractions should be considered mixing ages. The age of the finest fraction (12 ± 0.5 Ma, for <0.2 μm) is similar to that obtained by the theoretical simulation (11.37 Ma, based on thermo-stratigraphic evolution of the basin considering the model 5, Fig. 8) and could be interpreted as diagenetic and representative of the long-lived growth mechanisms within the basin. The age of *ca*. 21 Ma is compatible with the age of the populations identified from the U–Pb zircon analysis in the same level. This age is likely associated with a former volcanic episode that remobilized older zircons as well as volcanic glass at *ca*. 13 Ma. In that case, the ages obtained for the fractions analysed in TRT3 would be mixing ages between the two volcanic events and the ages of the mineral neoformation. The three main Andean volcanic episodes at *ca*. 5, 13 and 21 Ma interpreted from the U–Pb detrital ages, are consistent with the Late Oligocene to recent magmatic pulses reported along the Andean arc between 28.5 and 32.5 South Latitude (Kay & Mpodozis, 2002). Our detrital ages from the Vinchina Basin strata clearly testify the eastward shifting of magmatic activity from the Early Miocene (Furque, 1963; Jordan *et al.*, 1993; Limarino *et al.*, 2001; Vergés *et al.*, 2001; Kay & Mpodozis, 2002; Dávila *et al.*, 2004). This arc migration and widening has been associated with subduction shallowing since about 18 Ma (Kay & Mpodozis, 2002; Dávila *et al.*, 2004).

The AHe ages for the two volcaniclastic levels at the Vinchina Basin cannot be interpreted conventionally, i.e. to constrain the time, amount and rate of cooling/exhumation, given that they overlap (within the margin of error) with the ages obtained for the volcaniclastic level located at the top of the Vinchina Basin (Toro Negro Fm., *ca*. 5.25 Ma). The best-fit models for the AHe ages (Fig. 11) are compatible with the burial temperatures indicated by the occurrence of R0 in the deepest part of the basin. This is also consistent with an extremely cold lithosphere likely associated with a flat slab subduction regime (i.e. with no asthenopheric mantle heat contribution). Although in basin analysis low-geothermal gradients can also be attributed to variations in sedimentation/exhumation rates ("blanketing effect") or deformational processes, we favour a change in the subduction setting, from normal to transitional and flat, which would have refrigerated the lithosphere.

Finally, some questions arise from comparison between the two basins. Why does the thermal modelling in the Vinchina Basin indicate colder thermal conditions than those currently taking place where the slab is flat (Bermejo Basin)? Modelling of the Miocene evolution of Vinchina Basin that considered the thermal conditions proposed for the Bermejo Basin (Model 6, see Fig. 8), yielded basal temperatures and I/S evolution with depth that are not compatible with interstratified I/S identified in the two analysed sections. How fast do clay minerals respond to increased heat? Could the migration of the lithosphere be not recorded by clay minerals and apatites and it is possible that disordered R0 I/S phases persist even at temperatures higher than 165°C? Is it is possible that the thermal regime that currently affects the flat slab segment is not the same that would have taken place in the flat Miocene slab regions? Would this depend on variations in the characteristics of the lithosphere and/or the

geometry of the flat slab as it migrated over time? It could be also possible that the Bermejo Basin has not yet cooled down from the hotter stage as conductive loss of heat is slow. By contrast, the Vinchina Basin could be formed in a cold tectonic setting. Mantle heat flow contributions of around 11–15 mW m^{-2} have been estimated for cratonic regions (Mareschal & Jaupart, 2004; Furlong & Chapman, 2013). This contribution is comparable with the difference between surface heat flows estimated for the two basins. Moreover, changes of crustal heat production, due to the presence of different types of crust, could account for the observed heat flow variations. Alternatively, higher heat diffusion within the Vinchina Basin, associated with a thicker crust to the north (seismic tomography data, see Whitman *et al.*, 1996), could have taken place. All these questions remain to be answered.

CONCLUDING REMARKS

Our clay mineral dating (*ca*. 154–39 Ma) is older than the U–Pb sedimentation ages (<16 Ma). This reflects a mixture of diagenetic and detrital material, according with transformation of clay minerals that shows a progressive illitization but at low temperatures, with occurrence of R0 even at deeper levels. This is in agreement with the obtained AHe ages (3.3–7.4 Ma), which are younger than the depositional ages and with the thermochronologic modelling showing a long residence time (between 5 and 10 Ma) within the AHePRZ zone, and with isotopic analyses and the subsidence histories. The modelling and comparison of mineralogic, K–Ar and Rb–Sr isotopic and thermochronologic data allow us to predict a heat flow of *ca*. 26 mW m^{-2} for a flat subduction regime to the north (Vinchina Basin) between 8 and 3.4 Ma, and 42 mW m^{-2} since 9 Ma to the south (Bermejo Basin). This supports an extremely cold flat subduction thermal regime for both basins from the Miocene to present.

ACKNOWLEDGEMENTS

We are grateful to the Consejo Nacional de Investigaciones Científicas y Técnicas (PIP 2012-2014 – 012 201101 00626), the Secretaría de Ciencia y Tecnología de la Universidad Nacional de Córdoba (Secyt 2014-2015), the IIF Marie Curie 7mo Programa Marco and the Fundação de Amparo a Pesquisa do Estado de São Paulo (FAPESP grants 2010/52172-1; 2011/17754-0) for financial support of our Research Projects in Argentina. This is a GEO-SEDex – USP contribution n 06. We acknowledge the help of Drs. Koji Kawashita and Umberto Cordani, for their constructive discussion of the results during the research. The authors are also thankful for the help of Ivone e Helen Sonoki, Liliane Petronillo, Solange Souza, Roberto Siqueira, Artur Onoe, Dr. Pedro Kiyohara and Simone Spieche with the Isotopic, TEM and AEM analyses. We also thank the very constructive reviews and comments by Susanne Schmidt and an anonymous reviewer and the editorial recommendations that improved this work.

CONFLICT OF INTEREST

No conflict of interest declared.

SUPPORTING INFORMATION

Additional Supporting Information may be found in the online version of this article:

Appendix S1. Theoretical framework.
Appendix S2. U–Pb data.
Appendix S3. Whole rock mineralogy of levels analysed in the four sections.
Appendix S4. Chemical analysis of identified grains.

REFERENCES

Allen, P.A. & Allen, J.R. (2005) *Basin Analysis: Principles and Applications*. 2nd edn. Blackwell Publishing Ltd., Oxford 549 pp.

Anderson, M., Alvarado, P., Zandt, G. & Beck, S. (2007) Geometry and brittle deformation of the subducting Nazca plate, Central Chile and Argentina. *Geophys. J. Int.*, **171**(1), 419–434.

Arostegui, J., Sangüsa, F.J., Nieto, F. & Uriarte, J.A. (2006) Thermal models and clay diagenesis in the Tertiary-Cretaceous sediments of the Alava block (Basque-Cantabrian basin, Spain). *Clay Miner.*, **41**, 791–809.

Astini, R.A., Dávila, F.M., López Gamundí, O., Gomez, F., Collo, G., Ezpeleta, M., Martina, F. & Ortiz, A. (2005) Cuencas de la Región Precordillerana. In: *Frontera Exploratoria de la Argentina* (Ed. by G.A. Chebli, J.S. Cortiñas, L.A. Spalletti, L. Lagarreta, E.L. Vallejo), pp. 115–145. Instituto Argentino del Petróleo y del Gas, Buenos Aires.

Awwiller, D.N. (1993) Illite-Smectite formation and potassium mass transfer during burial diagenesis of mudrocks: a study from the Texas Gulf-Coast Paleocene-Eocene. *J. Sediment. Petrol.*, **63**, 501–512.

Barazangi, M. & Isacks, B.I. (1976) Spatial distribution of earthquakes and subduction of the Nazca Plate beneath South America. *Geology*, **4**, 686–692.

Bense, F.A., Wemmer, K., Löbens, S. & Siegesmund, S. (2014) Fault gouge analyses: K-Ar illite dating, clay mineralogy and tectonic significance—a study from the Sierras Pampeanas, Argentina. *Int. J. Earth Sci.*, **103**, 189–218. doi:10.1007/s00531-013-0956-7.

Borzotta, E., Mamaní, M. & Venencia, J. (2009) Preliminary magnetotelluric study of Ambato and Valle Fértil lineaments in Bermejo Basin and Sierra de Valle Fértil, San Juan, Argentina. *Acta Geod. Geophys. Hungarica*, **44**(2), 157–166. doi:10.1556/AGeod. 44.2009.2.2.

Brown, R.W., Summerfield, M.A. & Gleadow, A.J.W. (1994) Apatite fission track analysis: its potential for the estimation

of denudation rates and the assessment of models of long term landscape development. In: *Process Models and Theoretical Geomorphology* (Ed. by M.J. Kirkby), pp 23–53. Wiley, Chichester.

Carrapa, B., Hauer, J., Schoenbohm, L., Strecker, M.R., Schmitt, A.K., Villanueva, A. & Sosa Gomez, J. (2008) Dynamics of deformation and sedimentation in the northern Sierras Pampeanas: an integrated study of the Neogene Fiambalá basin, NW Argentina. *Geol. Soc. Am. Bull.*, **120**, 1518–1543.

Ciccioli, P.L., Limarino, C. & Marenssi, S.A. (2005) Nuevas edades radimétricas para la Formación Toro Negro en la sierra de Los Colorados, Sierras Pampeanas Noroccidentales, provincia de La Rioja. *Rev. Asoc. Geol. Argentina*, **60**, 251–254.

Ciccioli, P.L., Limarino, C.O. & Friedman, R. (2012) La edad de la Formación Vinchina: Su implicancia en la estratigrafía de la cuenca de antepaís del Bermejo. *1st Simposio del Mioceno-Pleistoceno del Centro y Norte de Argentina*. S.M. del Tucumán. Ameghiniana, **49**, 4–7.

Ciccioli, P.L., Marenssi, S.A. & Limarino, C.O. (2014a) Petrology and provenance of the Toro Negro Formation (Neogene) of the Vinchina broken-foreland basin (Central Andes of Argentina). *J. S. Am. Earth Sci.*, **49**, 15–38.

Ciccioli, P., Limarino, C.O., Friedman, R. & Marenssi, S.A. (2014b) New high precision U-Pb ages for the Vinchina Formation: implications for the stratigraphy of the Bermejo Andean foreland basin (La Rioja province, western Argentina*). J. S. Am. Earth Sci.*, **56**, 200–213.

Clauer, N. (2007) Isotope dating and tracing of clay minerals from low-temperature environments. In: *Diagenesis and Low-Temperature Metamorphism. Theory, Methods and Regional Aspects* (Ed. by F. Nieto & J. Jiménez-Millán) pp. 85–96. Seminarios de la Sociedad Española de Mineralogía 3, Spain.

Clauer, N.Y. & Chaudhuri, S. (1999) Isotopic dating of very low-grade metasedimentary and metavolcanic rocks: techniques and methods. In: *Low-grade Metamorphism* (Ed. by M. Frey, D. Robinson), pp. 202–226. Blackwell, Oxford.

Collo, G., Dávila, F.M., Nieto, F., Nóbile, J.C. & Astini, R.A. (2009) Interstratified illite/smectite in the Miocene Central Andean foreland: evolution of clay minerals under very low-paleogeothermal gradients. XIV International Clay Conference, Castellaneta Marina, Italy, p. 214.

Collo, G., Dávila, F.M., Nóbile, J.C., Astini, R.A. & Gehrels, G. (2011) Clay mineralogy and thermal history of the Neogene Vinchina Basin, Central Andes of Argentina: analysis of factors controlling the heating conditions. *Tectonics*, **30**, TC4012. doi:10.1029/2010TC002841.

Collo, G., Dávila, F., Ezpeleta, M. & Teixeira, W. (2014) U-Pb detrital ages on tuffaceous and sandstone levels from a Neogene thick foreland basin of the Central Andes of Argentina. *Comun. Geol.*, Especial I, **101**, 405–407.

Cordani, U.G., Kawashita, K. & Thomaz Filho, A. (1978) Applicability of the rubidium-strontium method to shales and related rocks. *Contrib. Geol. Time Scale AAPG Studies Geol.*, **6**, 91–117.

Cordani, U.G., Mizusaki, A.M., Kawashita, K. & Thomaz-Filho, A. (2004) Rb-Sr systematics of Holocene pelitic sediments and their bearing on whole-rock datings. *Geol. Mag.*, **141**, 233–244.

Coughlin, T.J. (2002) Linked origen-oblique fault zones in the Central Argentine Andes: The basis of a new model for Andean orogenesis and metallogenesis. Unpublished Thesis, University of Queensland.

Dávila, F.M. & Astini, R.A. (2007) Cenozoic provenance history of synorogenic conglomerates in western Argentina (Famatina belt): implications for Central Andean foreland development. *Geol. Soc. Am. Bull.*, **119**, 609–622.

Dávila, F.M. & Carter, A. (2013) Exhumation history of the Andean broken foreland revisited. *Geology*, **41**, 443–446.

Dávila, F.M., Astini, R.A., Jordan, T.E. & Kay, S.M. (2004) Early Miocene andesite conglomerates in the Sierra de Famatina, broken foreland region of western Argentina, and documentation of magmatic broadening in the south-central Andes. *J. S. Am. Earth Sci.*, **17**, 89–101.

Dávila, F.M., Collo, G., Astini, R.A. & Gehrels, G. (2008) U-Pb detrital ages on a tuffaceous sandstone sheet in the Vinchina Formation, La Rioja, Argentina: Deposition and exhumation implications. XVII Congreso Geológico Argentino, 95-96.

Ehlers, T.A. & Farley, K.A. (2003) Apatite (U–Th)/He thermochronometry: methods and applications to problems in tectonic and surface processes. *Earth Planet. Sci. Lett.*, **206**, 1–14.

Farley, K.A., Wolf, R.A. & Silver, L.T. (1996) The effects of long alpha-stopping distances on (U-Th)/He ages. *Geochim. Cosmochim. Acta*, **60**, 4223–4229.

Fitzgerald, P.G., Sorkhabi, R.B., Redfield, T.F. & Stump, E. (1995) Uplift and denudation of the central Alaska Range: a case study in the use of apatite fission track thermochronology to determine absolute uplift parameters. *J. Geophys. Res.*, **100**, 175–191.

Flowers, R.M., Ketcham, R.A., Shuster, D.L. & Farley, K.A. (2009) Apatite (U–Th)/He thermochronometry using a radiation damage accumulation and annealing model. *Geochim. Cosmochim. Acta*, **3**, 2347–2365.

Frey, M. & Robinson, D. (1999) *Low Grade Metamorphism*. Blackwell Science, Cambridge, 313 pp.

Furlong, K.P. & Chapman, D.S. (2013) Heat Flow, Heat Generation, and the Thermal State of the Lithoshpere. *Annu. Rev. Earth Planet. Sci.*, 05/2012. **41**, 345–410.

Furque, G. (1963) Descripción Geológica de la Hoja 17b. Guandacol (Provincias de La Rioja y San Juan): Buenos Aires, Argentina Dirección Nacional de Geología y Minería, Boletín 92.

Gillot, P.Y., Hildenbrand, A., Lefèvre, J.C. & Albore-Livadie, C. (2006) The K/Ar dating method: principle, analytical techniques, and application to Holocene volcanic eruptions in Southern Italy. *Acta Vulcanol.*, **18**(2006), 55–66.

Gutscher, M.-A., Spakman, W., Bijwaard, H. & Engdahl, E.R. (2000) Geodynamics of flat subduction: seismicity and tomographic constraints from the Andean margin. *Tectonics*, **19**, 814–833.

Hamza, V.M., Silva Dias, F.J.S., Gomes, A.J.L. & Delgadilho Terceros, Z.G. (2005) Numerical and functional representations of regional heat flow in South America. *Phys. Earth Planet. Inter.*, **152**, 223–256.

Hoke, G.B., Giambiagi, L.B., Garzione, C.N., Mahoney, J.B. & Strecker, M.R. (2014) Neogene paleoelevation of intermontane basins in a narrow, compressional mountain range, southern Central Andes of Argentina. *Earth Planet. Sci. Lett.*, **406**, 153–164.

Huang, W.-L., Longo, J.L. & Pevear, D.R. (1993) An experimentally derived kinetic model for smectite-to-illite conver-

sion and its use as a geothermometer. *Clays Clay Miner.*, **41**, 162–177.

Hunziker, J.C., Frey, M., Clauer, N. & Dallmeyer, R.D. (1986) Reply to the comments on the evolution of illite to muscovite by J.R Glasmann. *Contrib. Mineral. Petrol.*, **96**, 75–77.

Husson, L. & Moretti, S. (2002) Thermal regime of fold and thrust belts – an application to the Bolivian sub Andean zone. *Tectonophysics*, **345**, 253–280.

Johnson, N.M., Jordan, T.E., Johnsson, P.E. & Naeser, C.W. (1986) *Magnetic Polarity Stratigraphy, Age and Tectonic Setting of Fluvial Sediments in an Eastern Andean Foreland Basin, San Juan Province, Argentina, Foreland Basins*. (Ed. by P.E. Allen & P. Homewood). *Int. Assoc. Sedimentol.* 8, 63–75.

Jordan, T.E. & Alonso, R.N. (1987) Cenozoic stratigraphy and basin tectonics of the Andes Mountains, 20–28° South latitude. *Am. Assoc. Pet. Geol. Bull.*, **71**, 49–64.

Jordan, T.E., Allmendinger, R.W., Damanti, J.F. & Drake, R.E. (1993) Chronology of motion in a complete thrust belt: the Precordillera, 30°-31°, Andes Mountain. *J. Geol.*, **101**, 135–156.

Jordan, T.E., Schlunegger, F. & Cardozo, N. (2001) Unsteady and spatially variable evolution of the Neogene Andean Bermejo foreland basin, Argentina. *J. S. Am. Earth Sci.*, **14**, 775–798.

Kay, S.M. & Mpodozis, C. (2002) Magmatism as a probe to the Neogene shallowing of the Nazca plate beneath the modern Chilean flatslab. *J. S. Am. Earth Sci.*, **15**, 39–59.

Ketcham, R.A. (2005) Forward and inverse modeling of low-temperature thermochronometry data. *Rev. Mineral. Geochem.*, **58**, 275–314.

Ketcham, R.A., Carter, A., Donelick, R.A., Barbarand, J. & Hurford, A.J. (2007) Improved modelling of fission-track annealing in apatite. *Am. Mineral.*, **92**, 789–798.

Lanson, B. (1997) Decomposition of experimental X-Ray diffraction patterns (Profile fitting) a convenient way to study clay minerals. *Clays Clay Miner.*, **45**, 132–146.

Lencinas, R. (1994) Los depósitos pleistocenos–holocenos del valle de Famatina, La Rioja, Argentina. 7th Congreso Geológico Chileno 1, 465–470.

Limarino, C., Tripaldi, A., Marenssi, S., Net, L., Re, G. & Caselli, A. (2001) Tectonic control on the evolution of fluvial systems of the Vinchina Formation (Miocene), northwestern Argentina. *J. S. Am. Earth Sci.*, **14**, 751–762.

Ludwig, K.Ý. (2003) Isoplot/Ex, rev. 2.49. A Geochronological Toolkit for Microsoft Excel. Berkeley Geochronology Center, Special Publication No. 1a.

Mareschal, J.C. & Jaupart, C. (2004) Variations of surface heat ow and lithospheric thermal structure beneath the North American craton. *Earth Planet. Sci. Lett.*, **223**, 65–77.

Milana, J.P., Bercowski, F. & Jordan, T. (2003) Paleoambientes y magneto estratigrafía del Neógeno de la sierra de Mogna, y su relación con la Cuenca de Antepaís Andina. *Rev. Asoc. Geol. Argentina*, **58**, 447–473.

Moore, D.M. & Reynolds, R.C. (1997) *X-Ray Diffraction and the Identification and Analysis of Clay Minerals*. Oxford University Press, New York, 378 pp.

Nieto, F. & Abad, I. (2007) Clay-slate evolution. Onset of metamorphism. Invited Lectures. Proceedings of the 11th EUROCLAY Conference, Aveiro, Portugal 34-41.

Nóbile, J., Collo, G. & Dávila, F.M. (2008) Transformación progresiva de minerales de arcilla durante el soterramento de la cuenca de Vinchina (Mioceno Tardío-Plioceno), Sierras de los Colorados, La Rioja. XII Reunión Argentina de Sedimentología, Buenos Aires, 127.

Pevear, D.R. (1992) Illite age analysis, a new tool for basin thermal history analysis. In: Proceedings of the 7th International (Ed. by Y.K. Kharaka and A.S. Maest), 1251–1254. Symposium on Water-Rock Interactions, Park City, Utah.

Pevear, D.R. (1999) Illite and hydrocarbon exploration. *Proc. Natl Acad. Sci.*, **96**, 3440–3446.

Pollack, H.N., Hurter, S.J. & Johnston, J.R. (1993) Heat loss from the earth's interior: analysis of the global data set. *Rev. Geophys.*, **31**, 267–280.

Ramos, V.A. (1970) Estratigrafía y estructura del Terciario en la sierra de los Colorados (Provincia de La Rioja), República Argentina. *Rev. Asoc. Geol. Argentina*, **25**, 359–382.

Ramos, V.A. (1999) Los depósitos sinorogénicos terciarios de la región andina. In: *Geología Argentina* (Ed. by R. Caminos) Anales 29: 22, pp. 651–682. Instituto de Geología y Recursos Minerales, Buenos Aires.

Ramos, V.A., Cristallini, E.O. & Pérez, D.J. (2002) The Pampean flat-slab of the Central Andes. *J. S. Am. Earth Sci.*, **15**, 59–78.

Re, G.H. & Barredo, S.P. (1993) Esquema de correlaciones de las formaciones terciarias aflorantes en el entorno de las Sierras Pampeanas y la Precordillera Argentina. *XII Congreso Geológico Argentino y II Congreso de Exploración de Hidrocarburos*, 2, 172–179.

Reiners, P.W., Ehlers, T.A. & Zeitler, P.K. (2005) Past, present, and future of thermochronology. *Rev. Mineral. Geochem.*, **58**, 1–18.

Rettke, R.C. (1980) Probable burial diagenetic and provenance effects on the Dakota Group clay mineralogy, Denver basin. *J. Sediment. Petrol.*, **51**, 541–551.

Reynolds, J.H., Jordan, T.E., Johnson, N.M., Damanti, J.F. & Tabbutt, K.D. (1990) Neogene deformation of the flat-subduction segment of the Argentine-Chilean Andes: magnetostratigraphy constraints from Las Juntas, La Rioja Province, Argentina. *Geol. Soc. Am. Bull.*, **102**, 1607–1622.

Richardson, T., Ridgway, K.D., Gilbert, H., Martino, R., Enkelmann, E., Anderson, M. & Alvarado, P. (2013) Neogene and Quaternary tectonics of the Eastern Sierras Pampeanas, Argentina: active intraplate deformation inboard of flat-slab subduction. *Tectonics*, **32**, doi:10.1002/tect.20054.

Sant' Anna, L.G., Clauer, N., Cordani, U.G., Riccomini, C., Velázquez, V.F. & Liewig, N. (2006) Origin and migration timing of hydrothermal fluids in sedimentary rocks of the Paraná Basin, South America. *Chem. Geol.*, **230**, 1–21.

Srodon, J. (2007) Illitization of smectite and history of sedimentary basins. Proceedings of the 11th EUROCLAY Conference, Aveiro, Portugal, 74-82.

Środoń, J. (1981) X-ray identification of randomly interstratified illite-smectite in mixtures with discrete illite. *Clay Miner.*, **16**, 97–304.

Środoń, J. (1999) Extracting K-Ar ages from shales: a theoretical test. *Clay Miner.*, **33**, 375–378.

Środoń, J., Clauer, N. & Eberl, D.D. (2002) Interpretation of K-Ar dates of illitic clays from sedimentary rocks aided by modelling. *Am. Mineral.*, **87**, 1528–1535.

Stockli, D.F., Dumitru, T.A., McWilliams, M.O. & Farley, K.A. (2003) Cenozoic tectonic evolution of the White Mountains, California and Nevada. *Geol. Soc. Am. Bull.*, **115**, 788–816.

Tabbutt, K.D. (1986) Fission track chronology of foreland basins, in the eastern Andes: Magmatic and tectonic implica-

tions. Unpublished Thesis. Dartmouth College, Hannover, New Hampshire.

Thomaz-Filho, A. & Lima, V.Q. (1981) Datação radiométrica de rochas sedimentares pelíticas pelo método Rb-Sr. *Boletim Técnico. Da Petrobrás*, **24**(2), 109–119.

Turner, J.C.M. (1964) Descripción geológica de la hoja 15 c Vinchina (Provincia de La Rioja). In: Carta geológico-económica de la República Argentina Escala 1: 200.000. Dirección Nacional Geología y Minería. Boletín 100, 81 pp.

Uysal, I.T. (1999) Mineralogy and isotope geochemistry of anthigenic clay and carbonate minerals in Late Permian coal measures, Bowen Basin, Queensland: Implications for thermal and fluid flow history. Ph.D. thesis, University of Queensland, Brisbane, Australia, 253 pp.

Uysal, I.T., Glikson, M., . Golding, S.D. & Audsley, F. (2000) The thermal history of the Bowen Basin, Queensland, Australia: vitrinite reflectance and clay mineralogy of Late Permian coal measures. *Tectonophysics*, **323**, 105–129.

Van der Pluijm, B.A. & Haines, S.H. (2008) *Radiometric Dating of Brittle Fault Rocks; Illite Polytype Age Analysis and Application to the Spanish Pyrenees*. AGU, San Francisco.

Velde, B. & Vasseur, G. (1992) Estimation of the diagenetic smectite to illite transformation in time–temperature space. *Am. Mineral.*, **77**, 967–976.

Vergés, J., Ramos, E., Seward, D., Busquets, P. & Colombo, F. (2001) Miocene sedimentary and tectonic evolution of the Andean Precordillera at 31°S, Argentina. *J. S. Am. Earth Sci.*, **14**, 735–750.

Whitman, D., Isacks, B.L. & Kay, S.M. (1996) Lithospheric structure and along-strike segmentation of the Central Andean Plateau: seismic Q, magmatism, flexure, topography and tectonics. In: *Geodynamics of the Andes* (Ed. by J.F. Dewey & S.H. Lamb), pp. 29, Elsevier, Amsterdam.

Wolf, R.A., Farley, K.A. & Silver, L.T. (1996) Helium diffusion and low-temperature thermochronometry of apatite. *Geochim. Cosmochim. Acta*, **60**, 4231–4240.

Wolf, R.A., Farley, K.A. & Wolf, D.M. (1998) Modelling of the temperature sensitivity of the apatite (U-Th)/He thermochronometer. *Chem. Geol.*, **148**, 105–114.

Yañez, G.A., Ranero, C.R., von Huene, R. & Diaz, J. (2001) Magnetic anomaly interpretation across the southern central Andes (32–34°S): the role of the Juan Fernández Ridge in the late Tertiary evolution of the margin. *J. Geophys. Res.*, **106**, 6325–6345.

Zapata, T.R. & Allmendinger, R. (1996) Thrust-Front zone of the Precordillera, Argentina: a thick-skinned triangle zone. *Am. Assoc. Pet. Geol. Bull.*, **80**, 359–381.

Manuscript received 1 December 2014; In revised form 15 September 2015; Manuscript accepted 29 September 2015.